ELSEVIER International Journal of Mass Spectrometry and Ion Processes 157/158 (1996) 39–83

International Journal of Mass Spectrometry and Ion Processes

The non-neutral plasma: an introduction to physics with relevance to cyclotron resonance mass spectrometry

A.J. Peurrung*, R.T. Kouzes[1], S.E. Barlow

Environmental Molecular Sciences Laboratory, Pacific Northwest National Laboratory, Richland, WA 9935, USA

Received 17 September 1995; accepted 29 December 1995

Abstract

The non-neutral plasma has been used as a valuable experimental medium separately by a generation of physicists and chemists. This work provides an introduction to the field of non-neutral plasma physics and reviews those findings that apply to the practice of cyclotron resonance mass spectrometry. We begin with fundamental concepts and definitions and continue in the logical order with characterizations of the equilibrium state, transport to equilibrium, and lastly the modes and waves supported by an unneutralized charge cloud. Because the emphasis throughout is placed on an intuitive presentation of the physics with relevance specifically to mass spectrometry, numerous citations to more complete work are provided.

Keywords: Cyclotron resonance mass spectrometry; Non-neutral plasma physics

1. Introduction

Investigations of trapped ion phenomena are routinely conducted by both chemists and physicists; however, close communication between the various communities involved has generally been lacking. In particular, physicists studying non-neutral plasmas have, until recently, usually not communicated with the broader chemical community. The reasons for this lack of communication are mainly historical; each community has grown to maturity by attacking different problems and without realizing the close similarity between their activities. In addition, it is important that no introductory treatments of non-neutral plasma physics exist. This review should promote communication by discussing selected results from the field of non-neutral plasma physics and pointing out their application to the field of Fourier transform ion cyclotron resonance mass spectrometry (FTICR–MS).

Non-neutral plasma physics is the study of unneutralized collections of charged particles whose dynamics are at least partially the result of collective effects [1,2]. Most work in this field has therefore been concerned with charge clouds large and dense enough to be considered true plasmas. In its simplest form, non-neutral plasma physics can be regarded as the study of many-body effects in a system of charged particles. FTICR–MS, in contrast, has advanced tremendously without primarily considering those effects which arise either because of the finite spatial extent of a charge cloud, or because of

* Corresponding author.
[1] Present address: West Virginia University, Morgantown, WV 26505, USA.

0168-1176/96/$15.00 Copyright © 1996 Elsevier Science B.V. All rights reserved
PII S0168-1176(96)04395-9

its collective nature. Indeed, most of the theoretical analyses presently available for FTICR–MS involve single particle dynamics [3–12] or the cyclotron-averaged interaction of two point-like charged particles [13–17]. Although some collective phenomena such as the cyclotron and magnetron motions [18,19] have been studied, they have not yet been rigorously analyzed as the modes of a system consisting of a large number of individual particles. It is our hope that this review may motivate efforts within both communities to understand the behavior of charge clouds under conditions of common interest to both.

The methods and principles of non-neutral plasma physics are of use whenever some amount of space-charge is contained by electric and magnetic fields. Some of the primary applications for non-neutral plasma physics have been neutral plasmas [20,21], high-power microwave generators [22], free-electron lasers [23], particle accelerators [24], antimatter experiments [25,26], astrophysics [27], fluid mechanics [28,29], atomic and molecular physics [30,31], and ion chemistry [32]. Although FTICR–MS is used here as a standard example, this review should have a broader applicability as a general introduction to the physics of charge clouds and serve as an example of the application of non-neutral plasma physics to new areas. This work is a review of neither FTICR–MS nor of non-neutral plasma physics; for that we refer the reader to more complete sources [1,2,33–35].

The field of non-neutral plasma physics began as the study of electron space-charge flow. A number of devices including vacuum tubes [36], microwave magnetrons [22], ionization gauges [37], and ion pumps [38] were invented prior to 1960 and required the understanding and control of some type of electron beam. Trapping of an electron plasma in isolation was achieved by three groups between 1965 and 1975, although only the third trap built by Malmberg and deGrassie [39] was similar to the traps generally used today. The first two traps were designed as a toroid [40] and a magnetic mirror [41], and were used to confine only relatively energetic electrons. A number of the advantages of non-neutral plasma over conventional, neutral plasma became increasingly evident after 1975. Unlike a neutral plasma, a non-neutral plasma can exist at any temperature because recombination of ions and electrons does not occur. Additionally, a non-neutral plasma has an extraordinarily long lifetime, and therefore reaches a state of overall thermal equilibrium which can be carefully studied. A subtle but important advantage of a non-neutral plasma is that it both generates and responds to electric fields. By using applied electric fields, an experimentalist can modify the temperature, length, width, shape, location, and orientation of a non-neutral plasma with great versatility. Powerful non-destructive [42–44] and destructive [45,46] diagnostic tools can measure either image currents in the trap walls or the actual plasma charge, respectively, revealing much about the plasma. The non-neutral plasma, in short, is an ideal experimental system since it is stable, long-lived, and can be manipulated and measured with great ease.

A plasma is a "gas" of charged particles that exhibits collective behavior. It is unimportant whether or not the system is neutral overall. One of the most fundamental collective properties of any plasma is its ability to accomplish Debye shielding of applied electric fields. (This process is simply the gas phase analog to the electrostatic screening in electrolytes that is familiar to chemists from Debye–Hückel theory.) Shielding occurs as a result of the freedom that charged particles have in a plasma to move in response to electric fields. The distance over which this shielding occurs in commonly known as the Debye length, given by [47]

$$\lambda_D = \sqrt{\frac{\epsilon_0 T}{nq^2}} \tag{1}$$

where n is the particle density, T is the temperature in energy units, q is the particle charge, and

ϵ_0 is the permitivity of free space appropriate for the SI system of units that are used throughout this paper. The quantity λ_D will appear repeatedly in subsequent sections because it constitutes the basic length scale for collective effects in a plasma.

There are two quantitative criteria which serve to qualify a charge cloud as a plasma. First, that the typical dimensions of the system be larger than the Debye length,

$$\lambda_D < \rho_c, z_c \tag{2}$$

where p_c is the cloud radius and $2z_c$ is the cloud's axial length. For a completely unneutralized charge cloud, this criterion also implies that the electrical potential energy gained or lost by a particle as it moves from the center to the edge of the charge cloud be larger than the average kinetic energy of the cloud particles, i.e. that the electric field generated by the charge cloud itself be important. The second condition for the existence of a true plasma is simply that the number of particles within a Debye sphere must be large:

$$n\lambda_D^3 \gg 1 \tag{3}$$

This criterion additionally guarantees that the average kinetic energy of the particles in the system (T) is much larger than a typical potential energy of interaction between two nearest neighbors ($q^2 n^{1/3}/4\pi\epsilon_0$), i.e. that the system resemble a gas rather than a liquid or a solid [48–52]. Although the charge clouds used in experiments usually satisfy Eq. (3), conditions have become increasingly common where this criterion is violated. We discuss this issue near the end of Section 3.

Many of the insights into trapped ion behavior found in the non-neutral plasma literature do not require the existence of a plasma in the formal sense of Eqs. (1) and (2). This is so because of the strong, long-range nature of the Coulomb force. Due to small size and relatively low density, the charge clouds used in FTICR–MS often fail to meet the criterion given in Eq. (2), but as we shall discuss in detail in subsequent sections, this does not substantially affect their behavior. Indeed, much of the material in this review falls within the view of non-neutral plasma physics, but does not depend on Eq. (2) for validity. Those specific instances where the value of ρ_c/λ_D is of importance are clearly pointed out.

The many variations of the Penning trap design [53] developed for non-neutral plasma physics and FTICR–MS share the basic trait that they trap particles by combined action of a homogeneous magnetic field and an electrostatic potential well. Fig. 1 shows a typical trap used for FTICR–MS containing a single, centered charge cloud. The major families of trap designs have electrodes that are box-shaped (shown in Fig. 1), cylindrical [39,54], and hyperbolic [55,56]. Within each of the trap families, a variety of designs are possible with differing aspect ratios [57], potential well shapes [58,59], symmetry characteristics [60], or schemes for manipulation and detection of charged particle motion [61–63]. In both non-neutral plasma physics and FTICR–MS there has been some attempt to

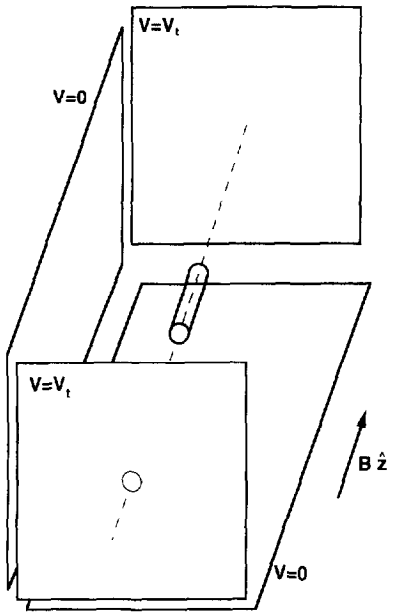

Fig. 1. Typical ion cyclotron resonance mass spectrometer cell containing a single charge cloud. The application of the trapping voltage V_t at the trap's ends and the axial magnetic field B combine to provide effective trapping. Two of the side-plates are not shown.

replace the electrostatic potential well with a ponderomotive potential well generated by oscillating potentials on the trap's endcaps [64–66], but this review will not treat the specific properties of these traps.

There are several important differences between the charge clouds traditionally studied in non-neutral plasma physics and the ion clouds used in mass spectrometry. An FTICR mass spectrometer can measure the charge-to-mass ratios of ions with masses from 1 u [67,68] to over 10^6 u [69–73], and charges greater than $30\,000e$ [74,75], where $-e$ is the electron's charge. In contrast, the "ions" usually used in non-neutral plasma physics are electrons, although work with atomic ions [76] and other, more exotic species such as positrons [25,77,78] has taken place. As we shall see, the factor of 10^9 between the masses of electrons and biomolecules is important for some situations. Another difference is that the charge clouds studied by the non-neutral plasma physics community generally consist of only one particle species. The charge clouds used in FTICR–MS, however, may contain more than one hundred different species. The large number of species may result from an impure sample such as crude oil [79,80], or from variations in the charge states and isotopic composition of large molecules [81,82]. A final important difference concerns cyclotron motion. The excitation of a cyclotron mode in which the entire trapped cloud rigidly undergoes a large-amplitude motion about the trap center is critical to FTICR–MS, yet is relatively unstudied [19] in non-neutral plasma physics. There have been several investigations of a mode in which the charge cloud rotates about its own center at approximately the cyclotron frequency [76,83,84], and numerous investigations of cyclotron mode phenomena [42,85–87]. However, less attention has been given to the specific phemonena associated with the long-term, center-of-mass cyclotron motion of one or more charge clouds about the trap center.

Our review should strengthen the relationship between FTICR–MS and non-neutral plasma physics by elucidating those results from non-neutral plasma physics which have some application within FTICR–MS. Whenever possible, both experimental and theoretical results from non-neutral plasma physics are provided for comparison. Section 2 discusses the motion of a single charged particle inside a Penning trap. Emphasis in this section is on a clear, unified discussion of the particle's various motions and the development of a logical and consistent notation for later use. This section also begins to investigate the effect of space charge on cloud dynamics. Section 3 defines and describes the equilibrium state of a trapped charge cloud. The equilibrium state of a particular charge cloud is shown to be a unique function of its temperature, electrical potential energy, and canonical angular momentum. Energy and mass transport caused by like-particle collisions, charge-neutral collisions, and external interactions are the subject of Section 4. Section 5 treats a variety of charge cloud modes and waves and their applications.

2. Fundamental dynamics

2.1. Single particle motion

An ion in free space with mass m and charge q gyrates around magnetic field lines with a frequency

$$\Omega = \frac{|qB|}{m} \tag{4}$$

where B represents the uniform magnetic field $\boldsymbol{B}$ and Ω is called the cyclotron frequency. This and all other frequencies are positive by convention. Note that this review employs "ion" as a synonym for any point-like charged particle including electrons as well as atomic and molecular ions. In addition to this gyration, an ion in free space travels with constant velocity along the magnetic field. The inside of a Penning trap

differs from free space in two important ways. First, there is a static electrical potential $\phi(\boldsymbol{r})$ which traps particles by establishing a potential energy well in the direction along the magnetic field. Unless otherwise stated, the Penning trap is assumed to be azimuthally symmetric and the magnetic field is assumed to be perfectly aligned with the trap's symmetry axis. We thus define a cylindrical coordinate system (r,θ,z) where z measures displacement along the trap axis, and r and θ are polar coordinates that describe the perpendicular plane. In an azimuthally symmetric trap, the magnetic field $\boldsymbol{B} = |B|\hat{\boldsymbol{z}}$ is perfectly aligned with the central axis of symmetry; together they define the unique, axial direction. In a special class of traps known as harmonic traps the potential assumes the form

$$\phi(r) = V_t \frac{(z^2 - r^2/2)}{2d^2} \tag{5}$$

where d is a characteristic length for the trap and V_t is called the trapping voltage. Note that the successful trapping of cations requires $V_t > 0$ while anions require $V_t < 0$. The calculated values of d for a variety of trap designs can be found in the literature [3,54]. Although Eq. (5) is not a necessary assumption for much of the physics discussed in this review, it conveniently simplifies much of the mathematics. In addition, the potential in a variety of non-harmonic traps (with the exception of very elongated traps) can be approximated by Eq. (5) near the trap center. The second difference between the inside of a Penning trap and free space is the existence of the conducting walls. The induced surface charge in these conducting walls (image charge) exerts a force which has some important consequences.

Particle motion is, of course, somewhat more complicated inside a Penning trap. A dynamical analysis, however, requires little more than a careful application of Newton's third law. Here and throughout this review we neglect relativistic and quantum mechanical effects; these effects are treated elsewhere [2,4]. The axial motion of a charged particle is governed by the equation

$$\frac{d^2z}{dt^2} = -\frac{q}{m}\frac{\partial\phi}{\partial z} \tag{6}$$

which for a harmonic trap simply describes the motion of a simple harmonic oscillator with frequency

$$\omega_z = \sqrt{\frac{q}{m}\left(\frac{1}{z}\frac{\partial\phi}{\partial z}\right)} \tag{7}$$

A trap with the potential given in Eq. (5) therefore has an axial oscillation frequency given by $\omega_z = \sqrt{qV_t/md^2}$. A particle that moves azimuthally with velocity $v_\theta = \omega r$ is subject to three forces. The magnetic force $(qv_\theta B)\hat{\boldsymbol{r}}$ opposes the electric force $(-q\partial\phi/\partial r)\hat{\boldsymbol{r}}$ and the inertial (pseudo) force $(mv_\theta^2/r)\hat{\boldsymbol{r}}$. Force balance therefore restricts the possible values of ω to those that satisfy the quadratic equation

$$m\omega^2 - qB\omega + q\left(\frac{1}{r}\frac{\partial\phi}{\partial r}\right) = 0 \tag{8}$$

given by

$$\omega = \frac{\Omega}{2} \pm \frac{\Omega}{2}\sqrt{1 - \frac{2\omega_z^2}{\Omega^2}} \tag{9}$$

when the trap is harmonic. When $\omega_z^2/\Omega^2 < 1/2$, there are two possible solutions representing a fast, cyclotron-like motion and a slow, drift-like motion [88,89]. The slow drift is commonly called magnetron motion and its frequency is therefore denoted ω_M (ω_- also occurs in the literature). The associated drift radius is denoted r_d for compatibility with later results. When $\omega_z^2/\Omega^2 \ll 1/2$, the inertial force can be neglected in Eq. (8) and ω_M assumes the approximate form

$$\omega_M \approx V_t/2|B|d^2 \tag{10}$$

The larger of the two frequencies in Eq. (9) approximates the experimentally observed resonant cyclotron gyration with radius r_c and is denoted ω_+. (Calculation of the exact gyration frequency requires an accounting for all radial forces as described below.) In an anharmonic

trap ω_+ and ω_M are not unique; they depend on a particle's radial position and axial oscillation amplitude. It is not only possible but often unavoidable that these two motions occur simultaneously [4]. Fig. 2 shows an ion executing rapid cyclotron motion at frequency ω_+ while simultaneously drifting slowly about the trap center at the magnetron frequency ω_M. The upper limit $\omega_z^2/\Omega^2 = 1/2$ for stable ion motion is known as the Brillouin limit [90] and is discussed in Section 3. At this limit both the fast and slow motions coalesce into a single, gyration-like motion. Note that for a single particle in a harmonic trap, both the relation

$$\Omega^2 = \omega_+^2 + \omega_z^2 + \omega_M^2 \tag{11}$$

and the relation

$$\Omega = \omega_M + \omega_+ \tag{12}$$

are exactly true when image charge can be neglected. Eq. (11) has been called the invariance theorem [4]. Both of these relations can be used to exactly calculate the free-space cyclotron frequency of a trapped particle on the basis of frequencies measured inside a trap. Another interesting observation is that the product $\omega_M\omega_+ = \omega_z^2/2$ is a quantity which also depends on an ion's charge-to-mass ratio but is independent of B.

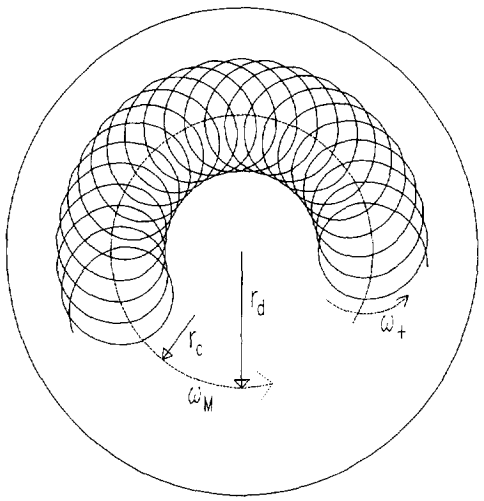

Fig. 2. Simultaneous magnetron and cyclotron motion. The ion undergoes rapid cyclotron motion with radius r_c and frequency ω_+ while drifting slowly around the trap center with the magnetron frequency ω_M and radius r_d.

The motion of a single particle within a charge cloud is qualitatively different from the motion of an isolated particle. The differences are directly due to the self-electric field of a non-neutral cloud. These effects are important even when Eq. (2) is not satisfied. The axial oscillation is either slightly or dramatically affected depending on the cloud's size and density. Additionally, the magnetron frequency no longer describes the actual frequency with which a charge cloud drifts around the trap's central axis. Similarly, ω_+ does not correspond to the experimentally observed cyclotron resonance frequency for a charge cloud. We also find an additional drift motion where the ions rotate about the cloud's central axis.

The axial oscillation frequency will certainly be reduced by the repulsive self-electric field of a charge cloud. In addition, since the potential from the charge cloud itself need not be harmonic, the total potential from the cloud and the trap may not be harmonic even when the trapping potential alone is. We can estimate the axial oscillation frequency if the charge cloud satisfies Eq. (2) and is therefore a true plasma. A plasma shields external potentials so that $\partial\phi/\partial z = 0$ within the plasma except in a narrow region at the plasma's edge [91], where ϕ includes both the trapping potential and the potential from the plasma. This axial shielding occurs within plasmas because charge is free to move in response to any potential differences that are present. In a plasma, therefore, an ion moves with a constant axial velocity except at the axial ends where it is rapidly turned around. The frequency with which an ion undergoes this motion is called the bounce frequency and has the approximate value

$$\omega_b = \frac{\pi v_z}{2z_c} \tag{13}$$

where v_z is the particle's axial speed and $2z_c$ is the plasma's axial length at the particle's (r,θ)

position. Section 3 discusses the length of a plasma and other issues concerning plasma shape.

A particle in a charge cloud acquires a slow, $\boldsymbol{E} \times \boldsymbol{B}$ drift rotation in the (r,θ) plane around the central axis of the charge cloud [19]. Cloud rotation is discussed more completely in Section 3 but is included here for the sake of a complete description of single particle motion. This rotation constitutes a fourth basic motion in addition to the cyclotron, axial, and magnetron oscillations that an isolated particle experiences. This rotation frequency can be calculated whenever the shape of the charge cloud is well known, but it can be quickly estimated only for particularly simple shapes. A true plasma in a harmonic trap has a spheroidal shape (see Section 3) with radius ρ_c in the (r,θ) plane and axial extent $2z_c$. The space charge from a cloud with this shape produces a radially outward electric field with the particularly simple form [3,85]

$$E = a(\alpha)\frac{m\omega_p^2}{q}r \tag{14}$$

where $\alpha = z_c/\rho_c$ is the cloud's aspect ratio, $a(\alpha)$ is a coefficient which accounts for the cloud's elongation, and r measures distance from the cloud center since the cloud is centered within the trap. The frequency, ω_p, is known as the plasma frequency and has the value

$$\omega_p = \sqrt{nq^2/\epsilon_0 m} \tag{15}$$

where n is the charge particle density inside what is assumed for simplicity to be a constant density cloud. In many applications such as this the plasma frequency represents a dimensionally convenient combination of parameters rather than an actual frequency of motion. The coefficient $a(\alpha)$ is obtained from

$$a(\alpha) = \frac{1}{2}\left(1 - \frac{1}{\alpha^2 - 1}Q_1^0\left[\frac{\alpha}{\sqrt{\alpha^2 - 1}}\right]\right) \tag{16}$$

where Q_1^0 is the associated Legendre function of the second kind. Fig. 3 shows a as a function of the cloud elongation. Note that Eq. (16) has two different forms valid when α is greater and less than one [3,85]. Since the electric field in Eq. (14) is proportional to r, $\boldsymbol{E} \times \boldsymbol{B}$ drift causes the cloud to rotate as a rigid rotor with a frequency

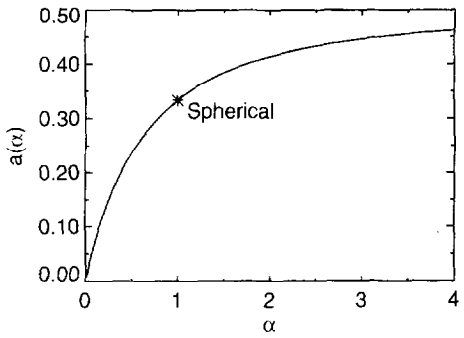

Fig. 3. Numerical coefficient a vs. α. The maximum value of 1/2 occurs for a cylindrically shaped charge cloud ($\alpha = \infty$) while a spherical charge cloud ($\alpha = 1$) has $a = 1/3$.

$$\omega_R = a(\alpha)\frac{\omega_p^2}{\Omega} \tag{17}$$

Note that Eq. (17) is strictly valid only for charge clouds that are significantly below the Brillouin limit ($\omega_R \ll \Omega$). A particular limiting case of Eq. (17) is of special interest. In an elongated trap or any trap with a particularly shallow potential well, the cloud's shape becomes very long axially and can be approximated as a cylinder whether it is a true plasma or not. In this limit $a(\alpha)$ approaches 0.5 and the rotation frequency becomes $\omega_R = \omega_p^2/2\Omega$.

The attraction between a cloud's space charge and its image charge in the trap walls causes a slow drift around the trap's central axis in addition to the magnetron drift caused by the trapping fields [3,92]. Although this drift exists even for a single trapped ion [93], it can generally be ignored unless the ion is highly charged. In conventional non-neutral plasma experiments, this image-induced drift is dominant and the motion it causes is called diocotron motion [94]. Diocotron and magnetron motions are actually quite similar; in one case the trapping potential causes drift, while in the other case it is the self-field of an off-center cloud [94]. Note

that there can be no such thing as pure magnetron or diocotron motion; both motions are always present for any charge cloud (see Section 5). We calculate the diocotron oscillation frequency for a cylindrical charge cloud below. The result for more realistic shapes is numerically similar but can be exactly calculated only by numerical computation. We assume for simplicity that the trap has cylindrical walls; the error from this assumption is large only when the charge cloud is so far off-center that it closely approaches the trap walls. With these assumptions, the image of a cloud at the position (r,θ) with linear charge density $\xi = \pi nq\rho_c^2$ consists of an oppositely charged column placed at the position $(r_w^2/r,\theta)$, where r_w is the wall radius [95]. Fig. 4 shows an end view of this image charge configuration. Together, the charge cloud and its image give rise to electric fields such that the trap's outer wall is on an equipotential contour. The image electric field at the charge cloud is approximately

$$E_r \approx \xi r/2\pi\epsilon_0 r_\omega^2 \tag{18}$$

where it is again assumed that the charge cloud is not close to the trap's outer walls so that $r/r_w \ll 1$. The diocotron frequency with which the charge cloud orbits the trap center becomes

$$\omega_D \approx \left(\frac{\rho_c^2}{r_\omega^2}\right)\omega_R \tag{19}$$

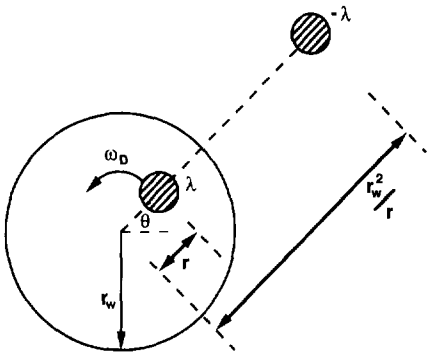

Fig. 4. Charge cloud with linear charge density λ at (r,θ) and its image at $(r_w^2/r,\theta)$. For this calculation, both the cloud and the trap are assumed to be cylindrical. The image electric field causes the charge cloud to drift around the trap center at the diocotron frequency ω_D.

Note that in this small-displacement limit ω_D is independent of amplitude. Whether ω_M or ω_D is larger for a particular charge cloud depends on the relative strength of the trapping and image electric fields.

The observed fast and slow oscillation frequencies that describe the motion of a single trapped particle must be revised when any additional forces such as an image charge force are present. These frequencies are obtained in the general case from an equation that is similar to Eq. (9), but includes the effect of an arbitrary radial force $F(r)$:

$$\omega = \frac{\Omega}{2} \pm \frac{\Omega}{2}\sqrt{1 - \frac{4}{m\Omega^2}\left(\frac{F(r)}{r}\right)} \tag{20}$$

For this more general situation the lower frequency is given approximately by

$$\omega_s \approx \omega_D + \omega_M + \text{other drifts} \tag{21}$$

where we have used ω_s to denote the frequency of this slow drift motion which includes magnetron drift, diocotron drift, and other drifts induced by radial forces. The fast cyclotron frequency is now denoted ω_{ICR} because it represents the experimentally observed cyclotron resonance frequency for the entire charge cloud. The invariance theorem (Eq. (11)) is no longer valid and cannot easily be revised because of the complicated nature of motion in a charge cloud. Provided that ω_M and ω_+ are replaced with ω_s and ω_{ICR}, Eq. (12) remains valid and becomes

$$\omega_{ICR} = \Omega - \omega_s \tag{22}$$

Eq. (22) can be verified by recomputing Eqs. (8) and (9) with the electric force $(q\partial\phi/\partial r)\hat{\mathbf{r}}$ replaced by an arbitrary radial force. The real power of Eq. (21) and Eq. (22) is that they can be extended to include several other causes of drift. Whatever electric fields combine to cause an off-center charge cloud to slowly drift around the trap center also reduce the frequency of the observed cyclotron resonance motion. Fig. 5 shows the three basic azimuthal motions which affect a charge cloud in a Penning trap. The cloud gyrates

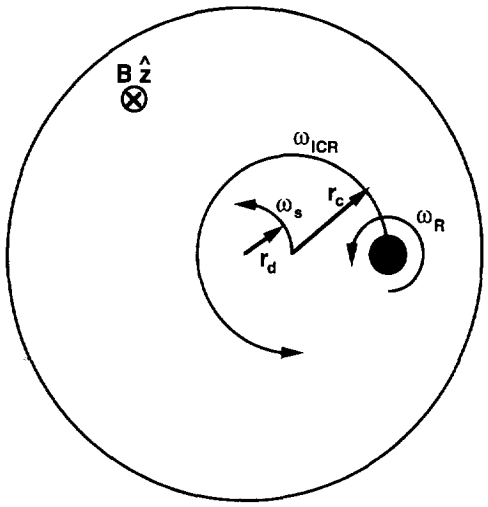

Fig. 5. Three basic azimuthal motions of a trapped charge cloud. The cloud rotates about its own center at ω_R, gyrates at ω_{ICR}, and drifts about the trap center at ω_s. All three motions must occur simultaneously. The drift and cyclotron radii are r_d and r_c, respectively.

at the ion cyclotron resonance frequency ω_{ICR}, rotates about its own center at the rotation frequency ω_R, and drifts around the trap center at the frequency ω_s. There is a fundamental similarity between the fast gyration and slow drift ion motions that arises because of their common origins in Eq. (9). Most statements applied to a particular type of motion are true also for the other motion in a specifically chosen frame of reference. This similarity is broken only by the fact that slow drift motion can occur only about the trap's central axis.

Table 1 summarizes the results of this subsection by listing the important dynamical frequencies for an isolated particle, and for a particle within a charge cloud.

A final note for this chapter concerns trap universality. Superficially, the dynamical frequencies depend on the specific features of each particular trap's design. At a deeper level, however, one finds that a substantial amount of charge cloud behavior is remarkably trap independent. All but very long traps have a potential structure that can be described by Eq. (2) with additional terms representing

Table 1
Important dynamical frequencies for a trapped ion both in isolation and within a charge cloud

Symbol	Formula	Name
Ω	$\lvert q\rvert B/m$	cyclotron
ω_M	$\approx V_t/2Bd^2$	magnetron
ω_z	$\sqrt{qV_t/md^2}$	axial
ω_+	$\Omega-\omega_M$	cyclotron-resonance
ω_b	$\pi v_z/2z_c$	bounce
ω_p	$\sqrt{nq^2/\epsilon_0 m}$	plasma
ω_R	$a(\alpha)\omega_p^2/\Omega$	rotation
ω_D	$\omega_R\rho_c^2/r_w^2$	diocotron
ω_s	$\approx \omega_D+\omega_M$	slow drift
ω_{ICR}	$\Omega-\omega_s$	cyclotron resonance

imperfections or irregularities. However, many imperfections take the form of a simple axial or radial force and therefore result in only a slight spatial shift of the trap's effective central point [96]. Further universality of trap behavior is likely the result of the various dynamically conserved quantities discussed in the following subsection.

2.2. Conserved quantities

This subsection presents a number of tools which are useful for the analysis of particle motion. Foremost among these tools are angular momentum conservation and energy conservation. Just as in simple mechanical systems involving roller coasters and inclined planes, the application of conservation laws to trapped particle motion often provides a shortcut, avoiding the need for a full solution to the equations of motion. In addition, this subsection reviews adiabatic invariants and their use for charged particle motion. The dynamics discussed in this subsection apply both to an individual trapped particle and to an entire cloud. Many aspects of charge cloud dynamics can be described by treating the cloud as a single particle whose charge and mass are simply the sum of the charge and mass of the constituent particles (see Section 5).

A secondary purpose of this subsection is to point out that the basic dynamics of trapped

charged particles are largely independent of the details of trap design. The importance of this point is suggested by the separate development of the various communities that utilize Penning traps in experimental work. The diocotron motion described above has been the subject of independent theoretical and experimental investigation within the FTICR–MS [3,12,92], fundamental physics [93], and non-neutral plasma [94] communities. One possible reason for this independence is that each group has historically favored a particular trap design and paid less attention to results achieved with other types of traps. For a number of years non-neutral plasma traps were cylindrical and highly symmetric [60] while FTICR–MS traps were often box-shaped [34]. It was with considerable surprise [97] that each community learned about results achieved with alternate trap designs. Both communities have recently begun to explore the possibility of alternate trap designs [56,98].

Every continuous symmetry in a dynamical system is associated with a conserved quantity. The conserved quantity associated with azimuthal symmetry in a Penning trap is the canonical angular momentum of a trapped particle

$$L_z = mv_{\theta r} + qr^2B/2 \tag{23}$$

which can be expressed in terms of the drift and cyclotron radii,

$$L_z = m\left(\omega_s \mathrm{sgn}(v_\theta) + \frac{\Omega}{2}\mathrm{sgn}(qB)\right)(r_d^2 - r_c^2) \tag{24}$$

where $\mathrm{sgn}(x) = x/|x|$. As can be seen from Eq. (23), the canonical angular momentum is simply the mechanical angular momentum $mv_\theta r$ plus a term that arises from the magnetic field. That there should be a magnetic contribution to the angular momentum is apparent from the fact that a changing magnetic field exerts a force $\boldsymbol{F}$ (and therefore a torque) on a charged particle according to

$$\nabla \times \boldsymbol{F} = -q\partial \boldsymbol{B}/\partial t \tag{25}$$

which is easily derived from Faraday's law and the Lorentz force equation. When $|v_\theta| \gg r\Omega/2$ (i.e. $r_d \gg r_c$), the second term in Eq. (24) is much larger than the first and the angular momentum can be written $L_z \sim qr^2B/2$. When $|v_\theta| \ll r\Omega/2$ (i.e. $r_d \ll r_c$), the ordinary kinetic angular momentum is dominant and we find that $L_z \sim -qr^2B/2$. The consequences of angular momentum conservation are explored in later sections.

The total energy of trapped charge is exactly conserved provided that the trapping fields are time independent and that all external interactions are ignored (see Section 4). Contributions to the energy of a single trapped particle arise from the electrostatic potential energy of the particle in the trap's electric field, the electrostatic potential energy of the particle and its image, the gravitational potential energy, and the kinetic energy of motion. Generally, the potential energy in the trapping fields is the largest component of total energy. Thus, as a particle undergoes magnetron motion around the trap's central axis, it merely drifts along contours of constant total energy as would be expected. For a very highly charged ion or a large charge cloud, the energy arising from the image charge becomes relatively large since this term varies as q^2. A charge cloud has an additional energy contribution from its internal electrostatic energy. Gravitational energy is negligible in almost all situations [96,99].

Adiabatic invariants have traditionally been of great use for the analysis of charged particle motion[100–102] since they describe quantities that are approximately conserved whenever certain parameters vary sufficiently slowly [103]. (The error in this approximation is exponentially small.) The most common example of an adiabatic invariant is the ratio of the energy to the frequency of a simple pendulum. Rigorous proofs of several of the assumptions that are commonly made for the analysis of charge clouds require the use of adiabatic invariants. Such assumptions include the neglect of axial motion

(the two-dimensionalization of cloud dynamics) and the guiding center approximation used for the analysis of relatively slow dynamics.

Because the gyration, axial oscillation, and drift motions usually occur on the widely differing timescales $\Omega_{ICR} \gg \omega_z \gg \omega_s$, three different adiabatic invariants can be derived for a charge cloud. The adiabatic invariant corresponding to the fast cyclotron motion is [102]

$$I_1 = \pi m v_\perp^2 / \Omega_{ICR} \tag{26}$$

where $v_\perp$ is the velocity perpendicular to the magnetic field, i.e. the cyclotron velocity. This invariant must be approximately conserved during the course of slower motions such as axial oscillation and drift. In fact, the only processes fast enough to effect a change in the value of I_1 are collisional interactions (Section 4) and r.f. excitation. The adiabatic invariant corresponding to the intermediate speed, axial oscillation is obtained from

$$I_2 = \oint m v_z \, dz \tag{27}$$

where v_z is the axial velocity and the integral is evaluated over one complete oscillation period. Any changes to the trapping fields which occur slowly compared with an ion's axial oscillation must approximately conserve I_2. The third adiabatic invariant corresponding to slow drift motion is simply the area enclosed by an ion's drift orbit [6,96],

$$I_3 \propto B r_d^2 \tag{28}$$

Any forces exerted on an ion or charge cloud that change slowly compared with ω_s^{-1} must approximately conserve the area of the drift orbit.

Conservation of angular momentum and energy severely constrain the possible dynamics of a single trapped ion or an entire charge cloud [104,105]. The existence of three adiabatic invariants further constrains much of the dynamics that occur on slower timescales. A large fraction of the problems that arise in trapped charge cloud dynamics can be simplified or solved with the aid of the techniques discussed in this subsection.

3. Static equilibria

Possibly the most important and unusual property of a non-neutral charge cloud is its tendency to closely approach an equilibrium state. It is this property more than any other that allows for highly repeatable experiments to be conducted with these devices. This property is also responsible for the stability of the ion cyclotron mode that allows such high quality mass spectra. A neutral plasma, in contrast, can never be simultaneously confined and in a state of thermal equilibrium.

This section characterizes the equilibrium condition of a trapped charge cloud in a variety of experimentally relevant limits. We discuss the equilibrium profiles for clouds that are axially very long (cylindrically shaped), very short (disk-shaped), and intermediate in length (spheroidal). The general characteristics of clouds that are infinitely cold ($T = 0$, $\lambda_D = 0$), very hot ($\lambda_D \gg \rho_c$), and intermediate in temperature ($0 \leq \lambda_D \ll \rho_c$) are also described. The characteristics of clouds with arbitrary shape and temperature can usually be estimated based on these limiting cases. Finally, we examine the equilibria appropriate for the charge clouds commonly encountered in FTICR–MS, namely, clouds containing multiple ion species and clouds containing very highly charged ions.

A more detailed treatment of thermal equilibrium is available from several sources [2,106–108] to which the reader is referred. Our necessarily qualitative treatment of this subject should serve partly as an introduction to these careful and more complete works. For a treatment of the evolution of non-equilibrium charge clouds toward thermal equilibrium, we refer the reader to Section 4.

3.1. Defining and categorizing equilibria

A charge cloud approaches a state of thermal equilibrium as its internal energy is distributed according to a Maxwell–Boltzman distribution

[109]; i.e. a time- and position-independent temperature must exist, and the other motions of the system must be rigid body motions of the system as a whole (free of internal shear). The latter part of the above definition implies that a sealed dewar of water can be at thermal equilibrium while located on an aircraft in flight. There are a number of different dynamical states in which a charge cloud can satisfy the above definition. For example, an ion cloud undergoing some of the motions that are normally considered modes may be at equilibrium in the formal sense of this description. These motions include magnetron or diocotron drift, cyclotron motion, and axial oscillations (Section 5). Note that an equilibrium need not be a state of minimum energy with respect to changes in the cloud shape or location. The approach of an isolated charge cloud to thermal equilibrium does not alter its total energy, but only redistributes that energy internally.

The above definition of thermal equilibrium can be recast in terms of three basic criteria that together guarantee that a charge cloud is at a true state of equilibrium. These conditions ensure that no change can occur in a cloud's physical or velocity–space distribution. First, the cloud must have a single temperature that is uniformly valid within the cloud. A cloud with different perpendicular and parallel temperatures resulting from axial cloud compression or expansion is not strictly at equilibrium even though the time over which these motions are coupled may become very long [110]. The single temperature requirement merely reflects the fact that thermal conduction can never be completely neglected in a trapped charge cloud.

The second condition essential for equilibrium is that once the cyclotron and axial motions are eliminated by averaging, the remaining two-dimensional motion in the plane perpendicular to the trap axis must take the form of rigid-body motion. That is, the cloud's flow can have no shear or divergence. This requirement for equilibrium reflects the fact that friction cannot be neglected, even though it is often small enough to ignore for the analysis of short-term dynamics. Several interesting consequences of this criterion are immediately apparent. A hollow charge cloud (one with a density hole at its radial center) cannot be at equilibrium state because it is not shear-free [29,111]. Additionally, a single charge cloud undergoing bulk cyclotron motion may be at equilibrium (more discussion below), but two clouds that collide as they undergo cyclotron motion at different frequencies ω_{ICR} and ω_{ICR}' cannot be. The divergence of the flow in the region where two clouds collide is obviously non-zero and therefore frictional effects must cause some long-term change to occur. Alternately, at any point where two colliding clouds overlap, the ions do not have a Maxwellian velocity–space distribution and cannot be at equilibrium. However, the collisional interaction between colliding clouds is often so weak that each cloud can be assumed to reach an equilibrium independent of the others.

The third condition that is necessary for charge cloud equilibrium is independence from most types of external interactions. Among the possible external interactions which prevent the formation of a true equilibrium are particle loss, ion–neutral collisions [112,113], energy dissipation in resistive walls [88,94], radiative energy loss [114], or interaction with time-dependent electric trapping fields arising from mechanical vibration or electrical noise. Clearly, any real experimental system suffers from these interactions to some degree, resulting in the observed finite confinement lifetime for a single trapped charge cloud [60] and damping of the ion cyclotron resonance mode. The effect of external interactions on a charge cloud are discussed in Sections 4 and 5. In this section we simply postulate the existence of an effectively isolated charge cloud as a simple, yet important special case. Under certain conditions there are several types of interactions that may take place while a charge cloud is at equilibrium. For example, any interaction that couples only to a cloud's

center-of-mass motion is allowable. A single species cloud may therefore undergo cyclotron excitation without substantially affecting its equilibrium properties. Another acceptable type of interaction is the coupling of a charge cloud to an external thermal bath. The important point here is that once a charge cloud reaches equilibrium, the time-averaged flow of angular momentum and energy between the charge cloud and the external world must cease. Note that the external excitation used in FTICR–MS may leave a cloud in a non-equilibrium state. Although an equilibrium should reform, in practice this is probably prevented by ion–neutral interactions (see Section 4).

A practical compromise must sometimes be reached for our definition of thermal equilibrium. The dynamics of a trapped charge cloud are sufficiently complicated that a number of equilibria may each be approximately valid on a particular timescale. (Is a uranium nucleus at equilibrium?) The neglect of external interactions in our definition of thermal equilibrium is in reality an experimental idealization. Although a number of external interactions may cause the cloud shape or temperature to acquire a slight time dependence, the cloud should at any moment be accurately described by the equilibrium profiles discussed below.

3.2. Mathematical description of equilibria

A simple mathematical description of thermal equilibrium requires several simplifying assumptions. As stated in Section 2, the trap is assumed to be azimuthally symmetric and to have a uniform magnetic field that is perfectly aligned with the trap's mechanical axis. The charge cloud is assumed to be axially centered and azimuthally symmetric. In addition, we neglect the magnetic field generated by the motion of the cloud's charge. (This is equivalent to an assumption of non-relativistic charge motion.) Quantum mechanical effects are ignored throughout this section, and the effects of strong ion–ion correlation and multiple ion species are deferred until the end of the section. For simplicity we arbitrarily choose $\boldsymbol{B} = -B\hat{z}$ and $q > 0$ so that ions drift and gyrate in the $+\hat{\theta}$ direction.

It is a basic principle of statistical mechanics that the distribution function can only depend on quantities that are conserved by a system's dynamics [115]. The two conserved quantities in a Penning trap are the canonical angular momentum

$$L_z = p_\theta r - m\Omega r^2/2 \tag{29}$$

and the energy

$$H = \boldsymbol{p}^2/2m + q\phi(r,z) \tag{30}$$

where $\phi(r,z)$ represents the total electrical potential (resulting from both the trap and the cloud). It is straightforward to show that any distribution function which depends on energy and angular momentum only through the linear combination $H-\omega_R L_z$ describes rigid-body motion. The quantity $H-\omega_R L_z$ can be written

$$H - \omega_R L_z = (\boldsymbol{p} - mr\omega_R\hat{\theta})^2 + \Phi(r,z) \tag{31}$$

where $\Phi(r)$ is an effective potential energy with the value

$$\Phi(r,z) = mr^2\omega_R(\Omega - \omega_R)/2 + q\phi(r,z) \tag{32}$$

The average azimuthal velocity (v_θ) for ions with a distribution function of the form $f(H-\omega_R L_z)$ is

$$\langle v_\theta \rangle = \frac{\int v_\theta f \, \mathrm{d}^3\boldsymbol{p}}{\int f \, \mathrm{d}^3\boldsymbol{p}} \tag{33}$$

$$= \omega_R r \tag{34}$$

which describes a rigid-body rotation with a frequency ω_R. A distribution function corresponding to thermal equilibrium must have the above form and a Maxwellian distribution of the ion kinetic energies:

$$\int = \frac{n_0}{(2\pi mT)^{3/2}} \exp\left(\frac{-(H - \omega_R L_z)}{T}\right) \tag{35}$$

where n_0 is the central ion density at the cloud center and T is measured in energy units. This

distribution function has been normalized so that the radial density profile can be written

$$n(r) = \int f \, \mathrm{d}^3\boldsymbol{p} \tag{36}$$

$$= n_0 \exp(-\Phi(r,z)/T) \tag{37}$$

Although the distribution function in Eq. (35) automatically satisfies the criteria for thermal equilibrium (uniform temperature, rigid-body motion, and time independence), additional information is needed before the cloud profile can be completely specified. The Poisson equation

$$\nabla^2\phi = -n(r,z)q/\epsilon_0 \tag{38}$$

relates the trap's potential to the charge distribution within the cloud, providing the information needed for a formal (and often numerical [43,91,107,116]) solution. Unfortunately, Eqs. (35) and (38) are highly non-linear in $\phi(r,z)$ and can only be solved for certain special cases (see below).

An alternate method for obtaining information about equilibrium profiles involves use of the macroscopic fluid description for charge dynamics [117]. This description uses an equation of continuity,

$$\nabla\cdot(n(r,z)\boldsymbol{v}) = 0 \tag{39}$$

and a force balance (Euler) equation

$$r\omega_R^2\hat{r} - \nabla P/m + (qn(r,z)/m)(\boldsymbol{E} + \boldsymbol{v}\times\boldsymbol{B}) = 0 \tag{40}$$

to determine $n(r,z)$ and ω_R, where $P = n(r,z)T$ is a scalar pressure. The forces included in Eq. (40) are the same inertial (pseudo), electric, and magnetic forces used in Section 2 to determine single particle motion along with a pressure force.

3.3. Cold equilibria

The limit of equilibria at $T = 0$ ($\lambda_D = 0$) provides a simple but experimentally relevant case that captures much of the essential physics for charge clouds whose size is large compared with a Debye length. We consider three specific examples of $T = 0$ equilibria, each of which can be described exactly in terms of an uncomplicated shape and radial charge density distribution. Fig. 6 contains drawings of the very long, very short, and intermediate length $T = 0$ clouds considered below.

3.3.1. Very long $T = 0$ equilibria

Infinitely long charge clouds are the most thoroughly studied because of both their historical relevance to ion and electron beam technology and their inherent simplicity. The cylindrical shape for this equilibrium follows from the observation that there are no trapping potentials and, therefore, that $\partial n(r,z)/\partial z = 0$ everywhere. One can easily show that a cylinder with constant charge density n_0 for $r < \rho_c$ satisfies the Poisson equation with a potential

$$\phi(r) = -qn_0r^2/4\epsilon_0 \tag{41}$$

inside the charge cloud. Note that since the electric field strength $E(r) = \partial\phi(r)/\partial r$ increases

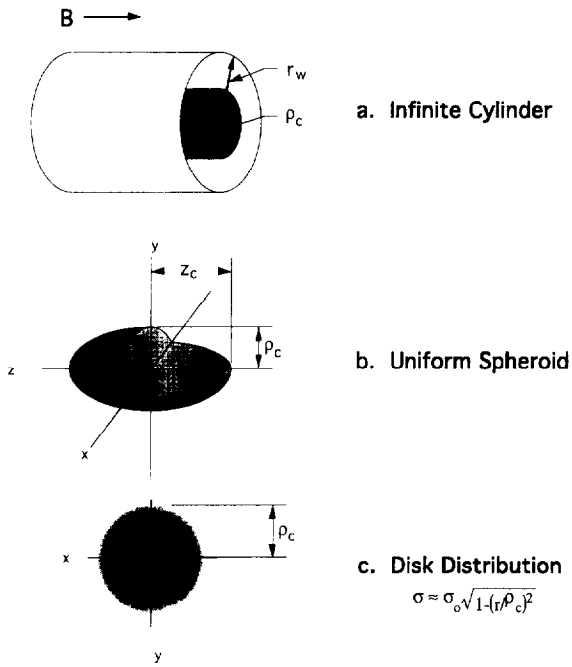

Fig. 6. Drawings of the three basic equilibrium shapes considered in this section.

linearly with radius inside the cloud, this solution automatically describes a cloud that rotates as a rigid-body. Inserting the above potential and density into the force balance equation (Eq. (40)) obtains the relation

$$m\omega^2 r - qB\omega r + (q^2 n_0/2\epsilon_0)r = 0 \tag{42}$$

that describes the possible rotation frequencies ω. Eqn (42) is readily solved to give

$$\omega = \frac{\Omega}{2}\left(1 \pm \sqrt{1 - \frac{2\omega_p^2}{\Omega^2}}\right) \tag{43}$$

Eq. (43) is very similar to Eq. (9) for the slow drift and fast gyration frequencies of a single particle, only with the single particle axial oscillation frequency ω_z replaced by the plasma frequency ω_p. We have again arrived at the Brillouin limit for charge confinement in a Penning trap. In Section 2, the limiting quantity was the radial trapping electric field, whereas here the limit is reached at $\omega_p^2 = \Omega^2/2$ because of the charge cloud's own electric field. Fig. 7 illustrates the possible rotation frequencies as a function of $\beta = 2\omega_p^2/\Omega^2$. The vast majority of charge clouds used in both FTICR–MS and non-neutral plasma physics satisfy $\beta \ll 1$ and lie on the lower branch of the curve in Fig. 7. The lower branch of this curve describes the slow, $\boldsymbol{E} \times \boldsymbol{B}$ drift rotation of the cloud about its own center, while the upper curve describes a cyclotron-like motion that is modified by the presence of radial electric fields. Although this fast rotation has been experimentally studied [76,84,87], it has no apparent application to FTICR–MS and is not considered further in this review. Near $\beta \sim 1$, these two motions become less and less distinct until at $\beta = 1$ the only possible motion is a rotation at the frequency $\Omega/2$ that is called Brillouin flow. As we shall see below, rotation at $\omega = \Omega/2$ is possible only in the limit of zero temperature.

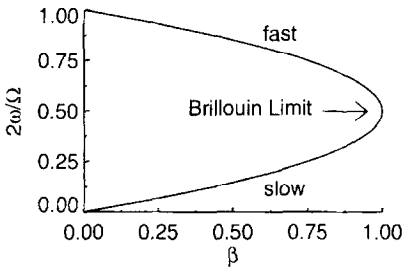

Fig. 7. Charge cloud rotation frequency ω as a function of β. The Brillouin limit corresponds to the point where $\beta = 1$. The upper branch of the curve where $\omega > \Omega/2$ is a fast, cyclotron-like mode of rotation. The lower branch where $\omega < \Omega/2$ is a slow, drift-like mode of rotation.

An experiment by Heinzen et al. [76] has demonstrated that the rotation frequency of a trapped ion cloud can be controlled by the application of a net torque (presumably with the limits $\omega_M < \omega < \omega_{ICR}$). Fig. 8 shows the clouds rotation frequency as a function of laser-induced torque exerted on the cloud. An extremely cold equilibrium is ensured in this experiment by the use of continuous laser cooling which reduces the cloud temperature below 250 mK. The hysteresis shown in Fig. 8 results from thermal effects and is discussed below. Eq. (43) predicts that the rotation frequency depends on β which in turn depends on the cloud density. This prediction was experimentally confirmed by the observation

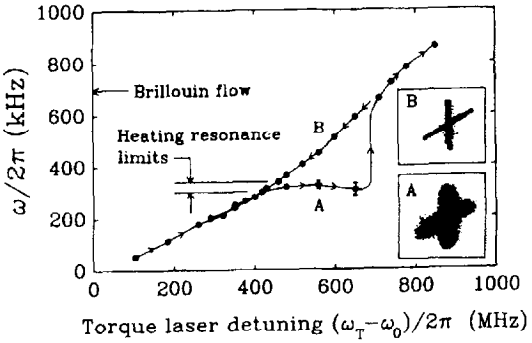

Fig. 8. Cloud rotation frequency as a function of torque laser frequency. An increase in the torque laser frequency causes an increase in the torque applied to the charge cloud that can only be balanced by "friction" at a higher rotational speed. Arrows indicate the direction of the frequency sweep. Insets A and B illustrate the appearance of hot and cold clouds, respectively. Image A was recorded on the lower branch of the hysteresis, and image B on the upper. Bright fluorescence from the cooling and diagonal beams, and weak fluorescence from the torque beam, is visible. This experiment was performed by Heinzen et al. [76].

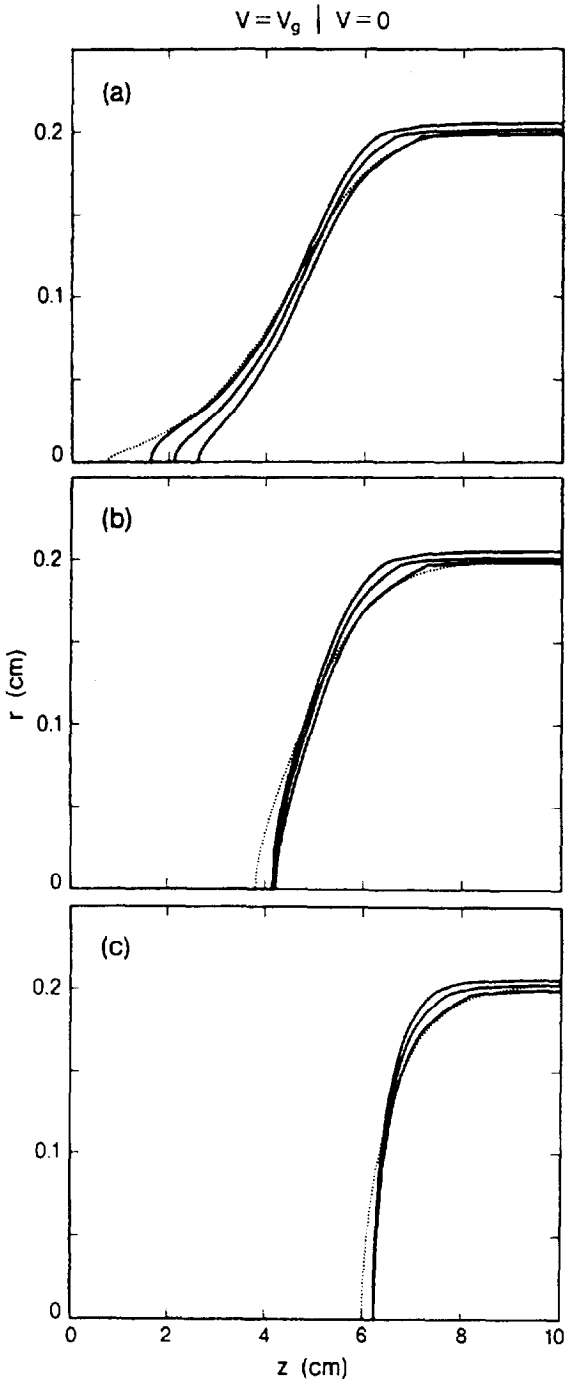

that for $\omega < \Omega/2$ an increase in torque compresses the plasma, while for $\omega > \Omega/2$ the opposite takes place.

In the $T = 0$ limit all three-dimensional charge clouds have constant density interiors with arbitrarily abrupt edges. (This can be understood from Eq. (37).) Complete specification of the equilibrium of long, cold charge clouds requires knowledge only of the shape of the cloud's outer boundary. To a good approximation, a long cloud has a central region that is approximately cylindrical and an outer region with a particular end-shape. This end-shape may depend on a number of parameters [43,91,107,116] including trap geometry, cloud radius and location, and the trap's confinement potential. A relatively simple analytic theory exists [91] for end-shape calculation and has been shown to provide approximate agreement with numerical shape calculations. Fig. 9 shows some representative possible shapes at one end of a long, cold charge cloud. An analytic theory also exists [116] that in many cases allows approximate calculation of the fully three-dimensional shapes of charge clouds that are displaced from the trap center because of magnetron or cyclotron motion.

For the special case of cold, infinitely long equilibria it is possible to drop the assumption of azimuthal trap symmetry. In the presence of asymmetric trapping fields, a cloud's equilibrium radial profile must acquire an azimuthal dependence. Although a cloud's charge must always rotate by drifting along equipotential contours, with trap asymmetry these contours are no longer circular. The shape of these contours can be calculated analytically [118,119] or experimentally measured by allowing the charge cloud to leave

Fig. 9. Numerical (solid) and theoretical (dotted) shapes of a single cloud with $\rho_c/\lambda_D = 27$ for three confinement voltages of (a) 104 V, (b) 125 V, and (c) 500 V. Solid lines show the locations at the charge cloud's edge where the density is equal to 20%, 50%, and 80% of the central density. Only one side of one end of a radially and axially symmetric plasma is shown. The confinement gate is to the left of the location indicated at $z = 5$ cm. This data is from Peurrung and Fajans [91].

the trap axially and measuring the amount of charge that arrives on each magnetic field line [46]. Fig. 10 shows the results of such an experiment. Based on these results, we expect that a charge cloud confined in a Penning trap with rectangular walls has a cross-section in the (r,θ) plane that is primarily circular, but has a slight perturbation of the form $\cos(4\theta)$.

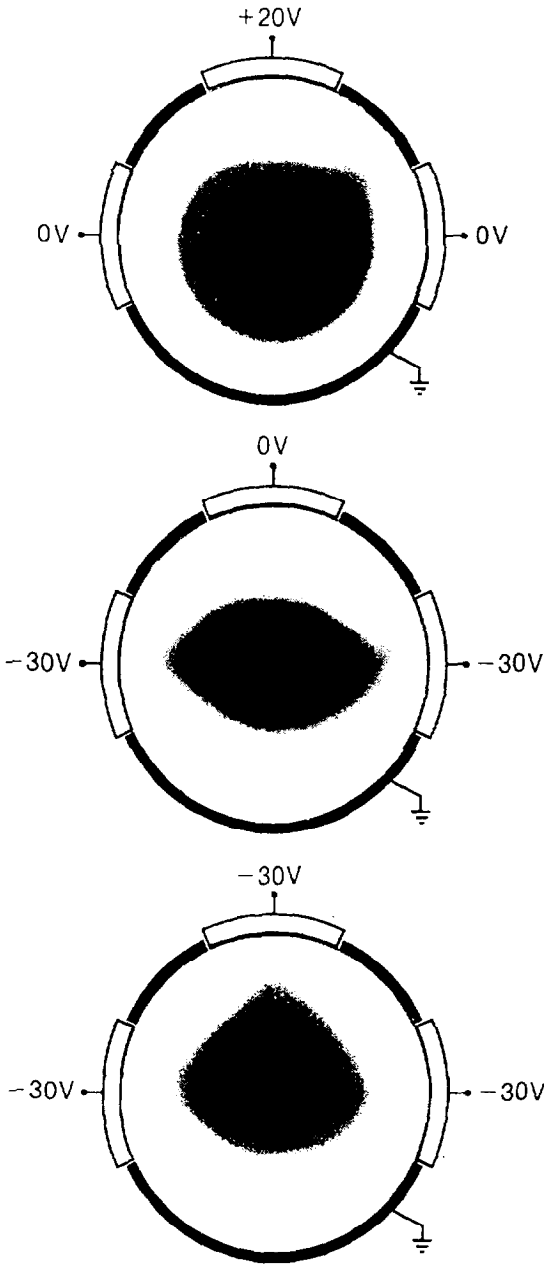

Fig. 10. Three experimentally observed non-circular cloud equilibrium shapes. These images are from Notte et al. [119].

3.3.2. Intermediate length $T = 0$ equilibria

In FTICR–MS, it is often reasonable to assume that the size of the charge cloud is small compared with the trap dimensions (z_c, $\rho_c \ll r_w$), and that the trapping potentials are harmonic. Under these conditions a notable simplification occurs in the solution for cold equilibria namely, the cloud takes the form of a constant density spheroid [3,120,121]. The aspect ratio $\alpha = z_c/\rho_c$ is found by requiring that the axial electric field E_z be zero within the plasma:

$$\left(\frac{m[1-2a(\alpha)]\omega_p^2}{q} - \frac{m\omega_z^2}{q}\right)z = 0 \tag{44}$$

where the two terms represent the field from the cloud [3,85] and the trap, respectively. The quantity $a(\alpha)$ was defined in Section 2 and is shown graphically in Fig. 3. A cloud's aspect ratio clearly depends on its charge density and the

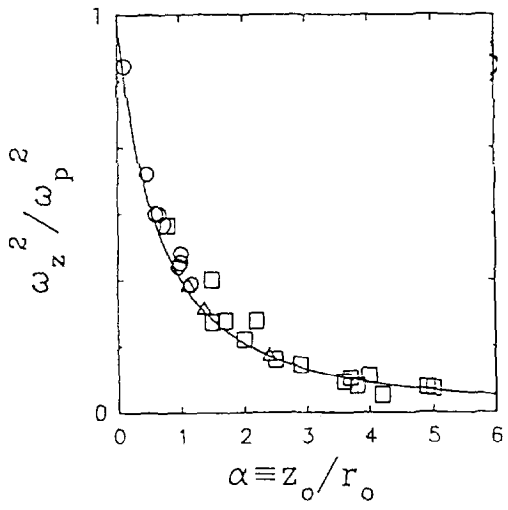

Fig. 11. Relationship between the cloud aspect ratio α and ω_z^2/ω_p^2 for spheroidal-shaped clouds in a Penning trap. The solid line is a theoretical curve from Eq. (44) with no adjustable parameters. The experimental measurements [120] were taken by Brewer et al. with two different traps at three different axial frequencies between $\omega_z/\Omega = 0.071$ and 0.121.

relative strength of the trapping field. Fig. 11 contains experimental aspect ratio measurements performed by Brewer et al. [120] for a wide range of shapes.

Calculation of the possible rotation frequencies for this equilibria proceeds in a manner similar to the calculations in Section 2 for single particle motion and the calculation above for cylindrical equilibria. The radial electric field within the spheroid

$$E_r = \frac{m\omega_z^2}{2q}r + \frac{ma(\alpha)\omega_p^2}{q}r \tag{45}$$

is inserted into the force balance equation (Eq. (40)), which is solved for ω to yield

$$\omega = \frac{\Omega}{2}\left(1 \pm \sqrt{1 - \frac{2\omega_p^2}{\Omega^2}}\right) \tag{46}$$

Note that Eq. (46) has a form that is identical to Eq. (43) for infinitely long, cylindrical equilibria. The Brillouin limit is again reached at $\beta = 2\omega_p^2/\Omega^2 = 1$. It is quite possible for routine experiments in FTICR–MS to approach the limiting condition $\beta = 1$. For example, a spherical cloud with $B = 3$ T, $\rho_c = 0.1$ cm, $q = 6e$, $m = 10^4$ u, $N = 2000$, and $V_t = 1$ V has $\beta = 0.2$.

3.3.3. Very short T = 0 equilibria

The equilibrium for axially very short clouds at $T = 0$ can be found by taking the limit of the spheroidal equilibrium as $\alpha \rightarrow 0$ and $\omega_p \rightarrow \infty$ in such a way that the total number of ions, N, is constant [122,123]. The resulting equilibrium is best viewed as a two-dimensional sheet with a charge distribution equal to that of a collapsed spheroid,

$$\sigma(r) = \sigma_0\sqrt{1 - r^2/\rho_c^2} \quad r < \rho_c \tag{47}$$

The radial electric field produced by this charge distribution is

$$E_r = \frac{3qN}{16\epsilon_0\rho_c^3}r \tag{48}$$

If desired, the rotation frequencies and Brillouin limit for this equilibrium can again be found using the force balance equation (Eq. (20)). Equilibria such as these would likely be encountered in applications with low temperatures and low charge density or in applications with large trapping potentials.

3.4. Finite temperature equilibria

This subsection describes equilibria with $T > 0$. The general characteristics of these equilibria depend primarily on the ratio ρ_c/λ_D (or z_c/λ_D). When $\rho_c/\lambda_D \gg 1$, the equilibria in all cases correspond closely to the appropriate $T = 0$ equilibrium except that the cloud's edge is no longer abrupt. A charge cloud at equilibrium in this regime always has an edge zone with a thickness (measured in the direction normal to the cloud boundary) that is of the order of λ_D. The appearance of this edge transition region results from the cloud's non-zero pressure; an overly abrupt edge would cause a large, outward pressure force at the cloud boundary, making rigid-body rotation impossible.

The appearance of this edge zone is most simply derived for the case of an infinitely long charge cloud. Neglecting the trapping potential and solving the Poisson equation (Eq. (38)) with the equilibrium density profile given in Eq. (37) yields the expected non-linear equation for $\phi(r)$:

$$\frac{1}{r}\frac{\partial}{\partial r}r\frac{\partial\phi(r)}{\partial r} = \frac{-qn_0}{\epsilon_0} \exp\left(-\frac{mr^2\omega_R(\Omega - \omega_R)/2 + q\phi(r)}{T}\right) \tag{49}$$

where the arbitrary choice has been made that $\phi(0) = 0$ ($\Phi(0) = 0$ follows from Eq. (32)). Before numerical solution, Eq. (37) is conveniently recast in the dimensionless form [107]

$$\frac{1}{s}\frac{\partial}{\partial s}s\frac{\partial\psi}{\partial s} = e^{\psi} - (\gamma + 1) \tag{50}$$

where $\Psi = -\Phi/T$, $s = r/\lambda_D$ is the scaled radius and

$$\gamma = \frac{2\epsilon_0 m\omega_R(\Omega - \omega_R)}{n_0 q^2} - 1 \quad (51)$$

is the only parameter that determines the radial density profile. Fig. 12 shows the radial density profile at thermal equilibrium computed from Eqs. (37), () and (50) as a function of the parameter γ. It is apparent that for $\rho_c \gg \lambda_D$ the thermal equilibrium density profile consists of a central region of approximately constant density and an edge region where the density decreases quickly to nearly zero over a distance of several λ_D.

A great deal of intuition can be gained by careful consideration of Eqs. (50) and (51). Clearly, a density profile $n(s)$ which decreases monotonically with s exists only for $\gamma > 0$. When $\gamma = 0$, Eq. (50) predicts that $n(s)$ remains constant (with the value n_0) as $s \rightarrow \infty$. This case corresponds to the cold equilibria discussed above; the condition $\gamma = 0$ is equivalent to Eq. (42) as long as $V_t = 0$. Thus, points lying on the parabolic curve in Fig. 7 correspond to cold equilibria, but points lying inside of the curve can only be attained at some finite temperature. The value of γ simply determines how close a particular equilibrium is to the limiting case of cold equilibrium. The experiment by Heinzen et al. [76] clearly demonstrates the transition from a cold equilibrium to a thermal equilibrium via resonant heating. The thicker appearance of the laser beams in inset A of Fig. 8 indicates a larger thermal motion of the cloud's ions. It can be shown for $\gamma \ll 1$ that the width of the charge column is $\rho_c \sim -\lambda_D \ln\gamma$ [108]. Note that ω_R cannot be determined from the charge cloud density alone as in the cold equilibrium case; here it depends additionally on the temperature T and scaled plasma radius ρ_c/λ_D. In fact, since the possible equilibrium profiles depend only on the single parameter γ, knowledge of any three of n_0, T, ρ_c, and ω_R is sufficient to determine the fourth.

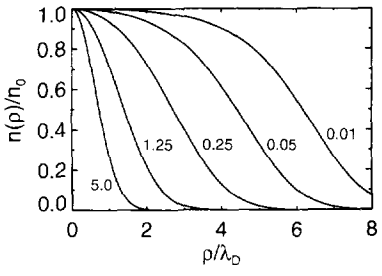

Fig. 12. Scaled density η/η_0 vs. scaled radius ρ/λ_D at thermal equilibrium for several values of the parameter γ. The values of γ for the indicated curves are 5.0, 1.25, 0.25, 0.05, and 0.01.

3.4.1. High temperature equilibria

A high temperature equilibrium forms whenever $\rho_c/\lambda_D \ll 1$, i.e. when the cloud size is much less than a Debye length. Such equilibria would be formed in FTICR–MS at either low cloud density or high temperature. In this limit, the ratio of the potential energy across the plasma radially, $q[\phi(\rho_c)-\phi(0)] = n_{0q}^2\rho_c^2/4\epsilon_0$, to the thermal energy T has the value $(\rho_c/2\lambda_D)^2$. The axial distribution of charge can therefore be calculated by neglecting the cloud's self-electric field:

$$n(r,z) = n(r)\exp[-q(\phi_t(r,z) - \phi_t(r,0))/T] \quad (52)$$

where $\phi_t(r,z)$ represents only the trapping potential. In other words, each ion in the cloud behaves as it would even if the rest of the cloud were not present.

The force balance equation (Eq. (40)) can again be used to require that these equilibria undergo rigid-body (shear-free) rotation. The radial density profile in Fig. 12 with $\gamma = 5.0$ shows the Gaussian shape that is typical of high temperature equilibria. For an infinitely long trap the cloud's radial profile approaches

$$n(r) = n_0\exp(-m\omega(\Omega - \omega)r^2/2T) \quad (53)$$

in the limit that $\rho_c/\lambda_D \rightarrow 0$, where ω is either of the two allowed rotation frequencies. Thus, high temperature equilibria have radial profiles that are nearly Gaussian. This result follows naturally from the discussion above that thermal equilibrium clouds have edge zones that are several λ_D wide; high temperature clouds consist entirely of edge.

3.5. Equilibria in FTICR–MS

The remainder of this section deals with the equilibria that may form under the conditions prevalent in FTICR–MS. We discuss specifically how the character of these equilibria may be affected by the presence of multiple ion species in the same charge cloud, and by the large ion charge and mass that frequently occur in mass spectrometric applications.

3.5.1. Centrifugal separation

It has been shown [124] that under some conditions the ions within a single cloud must centrifugally separate into distinct radial layers according to ion species. This separation occurs because of the slightly different radial forces experienced by ions of differing charge or mass as they drift around the cloud center. However, it can easily be shown that this should not normally happen to the clouds used in FTICR mass spectrometry. The criterion for substantial separation is that the difference in potential energy from the center to the outside of the cloud for various species must be comparable to or larger than the average ion thermal energy. Assuming that two ion species differ in mass by Δm but have the same charge q, the relevant ratio is

$$\frac{\Delta E}{T} \approx \frac{1}{T}\int_0^{\rho_c} \frac{\Delta m \omega_R^2 r \, dr}{2} \tag{54}$$

which is just the integral of the centrifugal force across the cloud. Upon evaluation of the integral and substitution for ω_R this ratio becomes

$$\frac{\Delta E}{T} \approx \left(\frac{\Delta m}{m}\right)\left(\frac{\omega_p^2}{\Omega^2}\right)\left(\frac{\rho_c^2}{\lambda_D^2}\right) \tag{55}$$

neglecting constant factors of order one. Since the first two terms in Eq. (55) are necessarily less than one and usually much less, and the third factor is seldom much greater than one, we conclude that centrifugal separation because of mass differences should almost never occur in FTICR–MS. A similar calculation shows that for ion species differing in charge by Δq this ratio becomes

$$\frac{\Delta E}{T} \approx \left(\frac{\Delta q}{q}\right)\left(\frac{\rho_c^2}{\lambda_D^2}\right) \tag{56}$$

which is also less than one in nearly all cases. If centrifugal separation were to occur, ions would become ordered from the center to the outside of the cloud in order of decreasing charge-to-mass ratio.

The presence of sufficiently strong, short-range interactions between ions can lead to an equilibrium state that is highly correlated. Such systems would exhibit an essentially liquid-like or even crystal-like behavior and therefore would not be true plasmas even when $\rho_c \gg \lambda_D$. Strong ion–ion correlation within an ion cloud may have important consequences during the excitation phase of FTICR–MS when a quiescent, centered ion cloud is forced to undergo cyclotron motion and fragment into less dense clouds each consisting of ions with a unique charge-to-mass ratio.

The strength of ion–ion Coulombic coupling is conveniently parameterized as the ratio of the typical potential energy between two nearby ions to the average thermal energy [48–52]

$$\Gamma = q^2/4\pi\epsilon_0 aT \tag{57}$$

where the average particle spacing a is defined via the relation $n = 1/(4\pi a^3/3)$. (An alternate way of interpreting this measure of correlation strength is as the number of ions within a Debye sphere, $n\lambda_D^3$.) When $\Gamma \ll 1$, the interaction energies are small enough that the ion cloud behaves as a ion "gas" and there is almost no correlation between the spatial positions of different ions. At $\Gamma \sim 2$, the onset of liquid-like behavior is expected; that is, a limited short-range order develops within the cloud. Crystallization should occur at $\Gamma \sim 180$ whereby long-range order develops and ion diffusion is greatly reduced [49,125–128].

According to Eq. (57) the three parameters that influence the degree of correlation in an ion cloud are the density, temperature, and ion charge. The

solid or liquid phases of an ordinary metal are highly correlated chiefly as a result of their very high density. Experiments in the field of non-neutral plasma physics have achieved Γ values of several hundred, but only with the aid of laser-induced cooling to a temperature of $T \sim 0.01$ K [50,52,129]. In an FTICR mass spectrometer, strong correlations are most likely to occur as a result of the potentially large ion charge q. An ion cloud with $q = 170e$ and $T = 300$ K should exhibit the same degree of correlation as an ion cloud with $q = e$ and $T = 0.01$ K. It is not only possible but also likely that the ion clouds formed by electrospray of very large biomolecules [74,75,81] are in the crystalline form.

Because of the limited number of ions that can be effectively cooled in a Penning trap, experiments with highly correlated equilibria have observed behavior that differs from the behavior expected in bulk liquids or solids. For example, both theory and experiment [50,52] have found that the ions separate into concentric shells (either cylindrical or spheroidal). At $\Gamma \sim 200$, ions are relatively free to diffuse within a single shell, but mobility between shells is nearly zero.

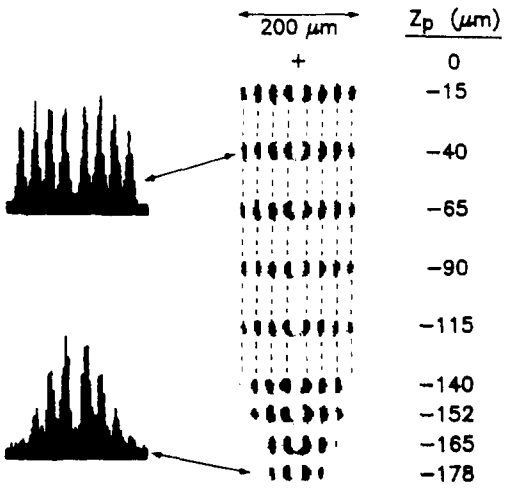

Fig. 13. Data from Bollinger et al. [129], showing evidence for cylindrical shells. On the right is a series of images obtained with the probe beam for different z positions z_p of the probe beam (lower half of the cloud only). Intensity plots for $z_p = -40$ μm and $z_p = 178$ μm are shown on the left. The cloud aspect ratio α was about 1.9 and $B \sim 1.92$ T.

Fig. 13 shows the experimentally measured profile of a highly correlated Be^+ ion cloud. The clearly visible shell structure is cylindrical in this case.

4. Non-equilibrium transport

Energy and mass transport are the fundamental processes governing the evolution toward thermal equilibrium of a trapped charge cloud. Energy transport is any process that causes a change in the velocity–space ion distribution $f(v)$ at some location within the cloud. For the purposes of this review, mass transport occurs via any process which changes the cloud's radial profile $n(r)$.

We divide transport phenomena into three categories depending on the associated cause. The first type of transport is caused by ion–ion collisions within a charge cloud. This transport causes thermal conduction, Maxwellianization of the ion velocity distribution, energy exchange between the degrees of freedom parallel and perpendicular to the magnetic field [20,110], and rearrangement of the radial profile [108,130–132]. Since ion–ion transport preserves the isolation of a charge cloud from the external trap, total energy and angular momentum must remain conserved. Generally, this type of transport is important for only a limited period of time as the cloud approaches its thermal equilibrium state. Ion–ion transport, therefore, occurs after formation or after any substantial change in the trapping electric fields.

Collisions between cloud ions and the neutral species that are inevitably present as a result of imperfect vacuum conditions cause the second type of transport. Because the cloud's total energy and angular momentum are not constrained, ion–neutral transport can cause a gradual expansion of the charge cloud that effectively limits the trapping time of a centered cloud [112,113,133], or the coherence time of a cloud that has been excited into the cyclotron mode

[19]. Indeed, control over this type of transport may be crucial for long-term cyclotron mode coherence in FTICR–MS.

The third type of transport results from a wide variety of external interactions. Any process by which a trapped ion cloud interacts with the outside world (excluding ion–neutral collisions) can cause external transport. Such processes include interaction with an external circuit, radial and axial particle loss, and interaction with time-dependent or asymmetric trapping fields. External transport is often unplanned and detrimental, but can also provide an additional means of controlling the properties of a trapped charge cloud. Both the cloud's total energy and its total angular momentum may fail to be conserved as a result of exchange with the external trap.

For each specific type of transport, it is usually necessary to know only whether it occurs quickly or slowly compared with a particular experimental phenomenon. For example, if one attempts to measure a particular reaction rate while using a FTICR mass spectrometer to detect reaction products, it is critically important that the ion cloud temperature be approximately constant during each measurement. The cloud temperature is approximately constant provided that thermal transport (of any particular kind) occurs either much slower than, or much faster than, the measurement time. If the transport is fast, then the cloud quickly reaches equilibrium and stays there during the measurement. If the transport is slow, then the cloud's temperature does not have sufficient time to undergo substantial change during the measurement. In many non-neutral plasma physics experiments it is standard practice to wait 5–10 s after cloud formation before any measurement commences so that any rapid transport is complete.

Due to the wide variety of ionic species and experimental conditions encountered in FTICR–MS, the relative speed of a particular kind of transport must be determined individually for each case. To this end, this section attempts to provide a number of approximate but easily utilized formulae describing transport along with an intuitive explanation of the physics of transport phenomena. Consequently, the emphasis is on a complete coverage of all possibilities rather than exactness. For a more thorough and exact treatment of transport, the reader is referred to the cited references.

4.1. Ion–ion transport

4.1.1. Ion–ion energy transport

Ion–ion transport of energy in a charge cloud may occur on two completely different time scales. The first and possibly faster of these two timescales is the timescale over which the plasma acquires well-defined but separate temperatures for the parallel and perpendicular (with respect to the trap's magnetic and mechanical axis) degrees of freedom. The second timescale governs the possibly slower process by which parallel and perpendicular energy are exchanged, allowing the two separate temperatures to coalesce into a single, globally applicable cloud temperature.

The temperature of any particular degree of freedom within a charge cloud is only defined when the velocity–space distribution of ions has a Maxwellian form ($f(p) \propto \exp(-|p^2|/2m_i)$). Any number of external manipulations may leave the cloud with a non-Maxwellian distribution. For example, there is no reason to expect that the cloud's distribution conforms to any particular form immediately after formation. The timescale for the formation of a Maxwellian distribution is set by the ion–ion collision rate [134]

$$\nu_{ii} \approx \frac{nq^4 \ln\Lambda}{2\pi\epsilon_0^2 m^2 \bar{v}^3} \tag{58}$$

where the Coulomb logarithm [134] typically satisfies $5 < \ln\Lambda < 10$ and $\bar{v}$ is the average ion velocity. Note that this collision rate can be rewritten (to within numerical factors of order one) as $\nu_{ii} \sim n\bar{b}^2\bar{v}$ where $\bar{b} = q^2/\epsilon_0 T_\parallel$ is the nominal distance of closest approach between two ions in a cloud with parallel temperature $T_\parallel$ (the temperature appropriate to describe the distribution of

axial kinetic energies). The second, simpler expression for the collision frequency is more intuitive since it takes the standard form: rate = density × cross-section × speed.

The formula for the ion–ion collision rate given in Eq. (58) is only a rough guide to the calculation of equilibrium timescales. Formulae for the more precise determination of relaxation rates for multispecies charge clouds containing ions of different masses, charges, or average energies are available in the literature [135]. Such formulae must be used for a number of real situations where the differences between colliding ions are substantial. For example, the process of sympathetic cooling discussed in Section 5 may involve the collision of heavy or highly charged ions with light ions or electrons. Other applications may require the collision of energetic ions with colder ions of the same species. In situations such as these, Eq. (58) may be seriously in error.

The ion–ion collision frequency always sets the rate for equipartition of energy within the various degrees of freedom within a charge cloud. Furthermore, if the Debye shielding distance λ_D is comparable to or less than the cloud's radius ρ_c, the temperature acquired by each degree of freedom is valid at all locations within the cloud. This occurs because ion–ion collisions effectively couple all ions that are within a distance λ_D of each other. Thermal conduction of heat across a cold, dense cloud with $\lambda_D < \rho_c$ is likely to take place on the slower timescale $(\lambda_D/\rho_c)^2 \nu_{ii}$ as long as collective processes do not act to speed energy transport.

The temperatures acquired by the parallel and perpendicular degrees of freedom after several collision times need not be equal. The timescale for exchange of energy between parallel and perpendicular degrees of freedom is set by both the ion–ion collision frequency ν_{ii} and the degree of magnetization of the charge cloud [20,110,136]. The magnetization parameter $\epsilon = \nu_{\|}/\Omega\bar{b}$ compares the fastest frequency associated with an ion's perpendicular motion (Ω) with the fastest frequency associated with parallel motion ($\nu_{\|}/b$). When $\epsilon \geq 1$, the cloud is weakly magnetized and ion–ion collisions lead to the free exchange of parallel and perpendicular energy. In this case the cloud acquires a single temperature during approximately the same time required for Maxwellianization of both the parallel and perpendicular velocity distributions. When $\epsilon \ll 1$, the charge cloud is strongly magnetized and an adiabatic invariant constrains the exchange of parallel and perpendicular energy [110]. In this case the equipartition of energy is slowed by the factor [136] $I(\epsilon) \sim 0.5\epsilon^{1/5}\exp(-2\epsilon^{-2/5})$. Note that this factor depends exponentially on ϵ, allowing the possibility that there may be very little exchange of parallel and perpendicular energy for very cold charge clouds in high magnetic fields.

A dramatic experimental measurement of equipartition rates as a function of charge cloud magnetization was performed by the non-neutral plasma group at U.C. San Diego [137]. Fig. 14 shows the parallel–perpendicular temperature relaxation rate as a function of the parameter ϵ. Both the weakly and strongly magnetized regimes are covered in this figure. These careful

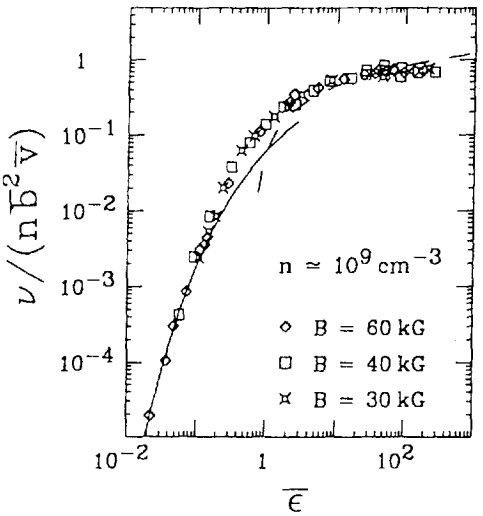

Fig. 14. Equipartition rate between parallel and perpendicular energy as a function of the magnetization parameter ϵ. The equipartition rate is normalized to the ion–ion collision frequency. This figure is taken from O'Neil et al. [137].

experiments proceed by first forming an electron plasma and allowing sufficient time for global equilibrium to be achieved. Subsequently, a one-dimensional axial compression (or expansion) is performed by deliberate alteration of the trapping potentials. Axial compression rapidly heats the parallel degree of freedom while approximately maintaining a Maxwellian distribution with a uniform parallel temperature throughout the cloud. The equipartition rate is obtained by measuring both the cloud's parallel and perpendicular temperatures at varying times after the compression. A cloud's parallel temperature can be measured via a well-controlled evaporation out of the axial ends of the trap [45]. The perpendicular temperature is measured by exploitation of the magnetic mirror effect [138].

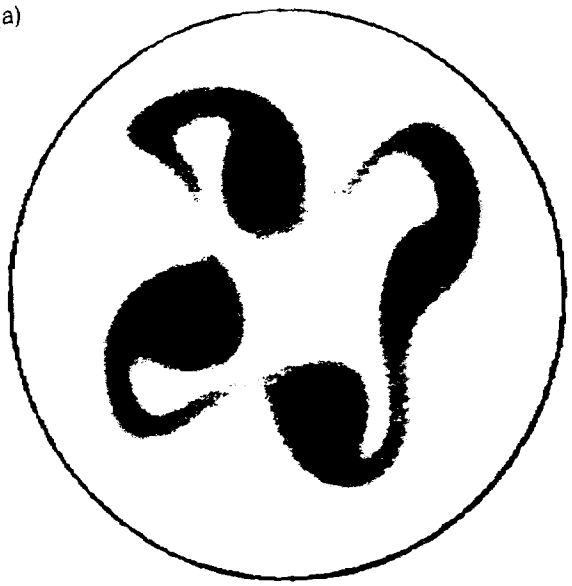

Fig. 15. Image of a cloud showing advanced diocotron growth. This image is from Peurrung and Fajans [29].

4.1.2. Ion–ion mass transport

Ion–ion mass transport in a charge cloud is rapid only when the charge cloud is subject to electrostatic instability. A sufficient condition for the electrostatic stability of a charge cloud is that its radial density profile $n(\rho)$ decrease monotonically with radius [139]. When this condition fails to be true, a slowly drifting charge cloud often undergoes the diocotron instability, causing rapid mass transport and bringing the cloud to a state such that the stability condition is satisfied [29,140]. Note that the causes and consequences of the diocotron instability are entirely different from the causes and consequences of the well-known diocotron mode (discussed in the next section). The primary similarity between the two is that both depend critically on the presence of some quantity of space-charge. The diocotron instability results from the shear that must be present in radially hollow charge clouds. An experimentally obtained, axial view [46] of a charge cloud that exhibits advanced growth of the diocotron instability is shown in Fig. 15. Although precise evaluation of the growth rate and consequent mass transfer timescale is complex, a rough magnitude can be estimated from the general nature of the process. Diocotron instability growth is a process that depends on space-charge induced drift, and therefore should occur at roughly the same rate as cloud rotation (ω_R) and diocotron mode motion (ω_D). In any case, this type of mass transport is relatively rapid, requiring much less than one second to effect a complete rearrangement of a cloud's radial profile [29,140].

The remaining types of ion–ion mass transport that act to bring a charge cloud toward its thermal equilibrium profile are all much slower than the instability-induced transport described above. The dominant mass transport mechanism depends strongly on the ratio of the Debye length λ_D to the typical thermal gyration radius $r_L = \Omega/\bar{v}_\perp$ where $\bar{v}_\perp$ is the average ion perpendicular velocity (excluding coherent motion such as the ion cyclotron resonance mode. The basic collisional steps for the cases $\lambda_D \leq r_L$ and $\lambda_D \gg r_L$ are shown in Fig. 16. When $\lambda_D \leq r_L$, ions separated by more than r_L do not interact strongly as a result of shielding and the collisions are direct. The head-on collision shown in Fig. 16 is actually a rarity shown only for simplicity—the

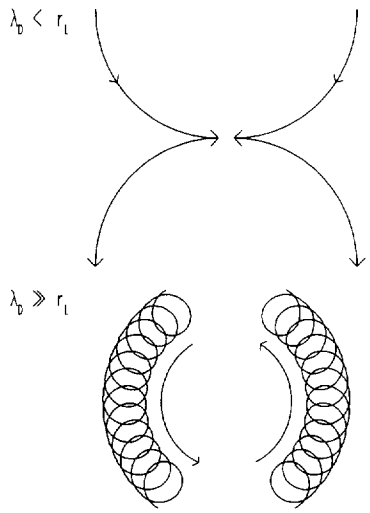

Fig. 16. Ion motion during the basic mass transport "step" for the two different mechanisms that are important when $\lambda_D \leq r_L$ and $\lambda_D \gg r_L$.

important point is that the collision occurs quickly compared with a cyclotron period. The rate at which a charge cloud approaches equilibrium via this mass transport mechanism is given by [108]

$$\nu = \frac{3}{8}\left(\frac{\omega_p}{\Omega}\right)^4 \nu_{ii} \tag{59}$$

where ω_p is the plasma frequency defined in Section 2. Since a charge cloud confined in a Penning trap must be below the Brillouin limit, it is generally true that $\omega_p \ll \Omega$ and the mass transport rate is much slower than the energy transport rate. In the alternate case when $\lambda_D \gg r_L$, ions undergo a cyclotron averaged interaction also shown in Fig. 16. In essence, these ions do not collide but instead slowly drift around their common center of mass. The mass transport rate in this case is enhanced by a factor of roughly $(\lambda_D/r_L)^2$ [130], but is still slow compared with the energy transport rates. An additional transport mechanism faster than either of the previous two has been theoretically predicted and experimentally verified [131,132]. This mechanism is important only for a special class of non-monitonically decreasing radial density profiles that are not subject to the diocotron instability. This type of radial density profile may occur in FTICR–MS as a result of axial ion loss from the cloud center as discussed later in this section.

4.2. Ion–neutral transport

Whether deliberate or inadvertent, the presence of a background neutral gas often has an important effect on the development of trapped charge clouds. There is an interesting analogy between the role of ion–neutral collisions in plasma physics and the role of ion–ion collisions in FTICR mass spectrometry. To a non-neutral plasma physicist, a Penning trap provides an ideal environment for the study of space-charge effects while ion–neutral interactions are a complicating effect to be avoided if possible and simply accounted for if necessary. In the chemical physics community, however, the Penning trap is an excellent medium for the carefully controlled study of ion–neutral interactions, while space-charge effects are often undesirable. In any experiment, it is important to consider the effects described here and to systematically account for them in the interpretation of experimental data.

As described below, ion–neutral interactions (collisions) may be an important or even primary cause of changes in the size, temperature, radial profile, and even composition of charge clouds. Several non-neutral plasma experiments have demonstrated the need for simultaneous measurement and control of neutral gas backgrounds whenever a charge cloud is trapped for an appreciable length of time [32,141,142]. In addition, collisional mode damping is currently a common technique in FTICR–MS [143–146]. Our treatment serves only as a brief outline of known phenomena; the reader is referred to the literature [32,135,147–154] for additional detail and insight.

4.2.1. Collision frequency

Central to the interpretation of collisional effects are the ion–neutral collision rate ν_{in} and

the ion–neutral collision cross-section σ_{in} which are related to each other by

$$\nu_{in} = n_n \int_0^\infty \sigma_{in} \upsilon f(\upsilon)\, d\upsilon \tag{60}$$

where υ is the relative speed, n_n is the neutral species density, and $f(\upsilon)$ is the joint ion–neutral speed distribution. The simplified form of Eq. (60),

$$\nu_{in} = \sigma_{in} \bar{\upsilon} n_n \tag{61}$$

where $\bar{\upsilon}$ is the average speed, is frequently satisfactory as a rough approximation for our purposes.

The collisional cross-section σ_{in} generally depends on the specific properties of the neutral species and the collision energy. Long-range interactions are normally of dominant importance for the moderately low energy collisions commonly encountered in FTICR–MS. Experimental evidence suggests that the overwhelming majority of observed effects can be accounted for by consideration of ion-induced dipole and ion–dipole interactions. (Higher order terms such as polarizability anisotropy and ion–quadrupole interactions do not appear to be important [150].) The collision rate between ions and non-polar neutral species is given by [147]

$$\nu_{in} = q\sqrt{\frac{\pi}{\epsilon_0}} \left(\sqrt{\frac{\alpha}{\mu_{in}}} \right) n_n \tag{62}$$

where q is as usual the ionic charge, α is the polarizability, and μ_{in} is the ion–neutral reduced mass. Note that in this equation and the next the charge q is measured in Coulombs instead of the more usual esu. In order to use q in esu, the factor $\sqrt{\pi/\epsilon_0}$ must be replaced by 2π. The frequency given in Eq. (62) is known as the Langevin rate after its discoverer.

Collisions with neutrals possessing permanent dipole moments have been successfully treated only more recently. In seminal work in 1973 [149], Su and Bowers describe the development of their average dipole orientation model (ADO) summarized by

$$\nu_{in} = q\sqrt{\frac{\pi}{\epsilon_0}} \left(\sqrt{\frac{\alpha}{\mu_{in}}} + cd\sqrt{\frac{2}{\mu_{in}\pi kT}} \right) n_n \tag{63}$$

where d is the permanent dipole moment, $c(d,\alpha)$ is a tabulated numerical scaling factor, and T is a temperature that can be roughly taken as the larger of the ion and neutral species temperatures. These authors found that the addition of a term proportional to the dipole moment, d, and inversely proportional to the square root of the temperature led to a major improvement in the interpretation of experimental data. This treatment has become a standard in the ion–molecule chemistry community.

Experimental observations indicate that the ADO treatment breaks down for neutral species that possess large dipole moments ($d > 1.5D$). The variational transition state theory (VTST) by Chesnavich et al. [151] and the statistical adiabatic theory (SAT) due to Troe [153] have been proposed for this regime. Although these treatments are physically different and produce formula with very different forms, both give similar results and are improvements over the earlier ADO treatment. (Both treatments break down in the limit of small dipole moments at which point one is obliged to employ ADO.)

Long-range forces are no longer dominant when the collision energy becomes large. The most appropriate model in this case is the hard spheres model described by

$$\nu_{in} = \sigma_{in}^{hs} \bar{\upsilon} n_n \tag{64}$$

where σ_{in}^{hs} is the hard spheres collision cross-section. This cross-section is generally a weak function of energy and can be estimated from either known or calculated Van der Waals' radii. For intermediate energy collisions, the larger of the two collision rates calculated via the polarization and hard spheres models is generally more accurate. The collision energy at which these two models agree can be roughly estimated as the polarization well depth; i.e. only

for collision energies exceeding the polarization well depth should it be necessary to use the hard spheres model. The transition between these two models is generally smooth and little difficulty is encountered.

The polarization models for ion–neutral collisions may also break down for very low energy collisions, although we can offer no simple formula valid in this region. At the very low energies now reached by some experimenters, ion–neutral collisions may take on a decidedly quantum mechanical nature. The only discussion we are aware of in the literature on this matter is by McDaniel [154], who considered the quantum mechanical ion-induced dipole interaction. An additional and potentially more serious limitation to the polarization models occurs for ions with a substantial internal structure. Recent developments in ion sources allow experimenters to introduce ions with masses greater the 10^7 u and charges greater than 10^4 e [74,75]. It is an open question whether any of the existing treatments applies to these large, structured ions.

4.2.2. Macroscopic effects

The macroscopic effects of ion–neutral collisions are simplest when the collisions are elastic. Elastic collisions produce the same basic types of energy and mass transport discussed elsewhere in this section for both internally and externally induced transport. (Ion–neutral transport is arguably a type of external transport, but we consider it as a separate category.) Inelastic collisions, in contrast, are able to effect a much wider variety of changes within a charge cloud. For example, inelastic collisions may also cause excitation or relaxation of an ion's internal modes, collisional dissociation, gas-phase chemical reactions, charge exchange, or other more complex processes. Treatment of these phenomena is specific to each situation, and shall not be dealt with further in this review.

Because a trapped charge cloud rotates at a frequency ω_R, it must experience a drag torque as a result of the presence of a background neutral gas. This torque changes the angular momentum of the charge cloud, causing it to undergo a slow radial expansion. The resulting decay of the cloud's central density has been modeled by Douglas and O'Neal [113] and experimentally tested by deGrassie and Malmberg [141]. The following model well describes the cloud's density decay:

$$n(r=0,t)=n(r=0,0)/(1+t/\tau_m) \tag{65}$$

where the decay time constant can be written

$$\tau_m=\frac{\Omega}{2\omega_R v_{in}}\frac{\mu_{in}}{m_i} \tag{66}$$

Eq. (66) contains two important generalizations upon the previous work that ensure applicability to both electron and ion clouds. First, the ratio of reduced mass μ_{in} to ion mass m_i accounts for the weakened effect of collisions for the ions whose mass is no longer negligible compared with the mass of the neutral species [148]. Second, τ_m is expressed using the cloud's rotation frequency instead of its plasma frequency. This change ensures that Eq. (66) remains correct for clouds of arbitrary shape and for clouds trapped in such a way that magnetron drift makes a substantial contribution to the rotation frequency. The cloud's rotation frequency properly belongs in Eq. (66) because the density decay is fundamentally a mobility process rather than a diffusive process.

The temperature of a trapped charge cloud is also directly affected by collisions with a background neutral gas. The rate at which the cloud's temperature relaxes to that of the background gas is given by

$$\frac{dT_i}{dt}=(T_n-T_i)\frac{2m_i m_n}{(m_n+m_i)^2}v_{in} \tag{67}$$

where T_n and T_i are the neutral and ion temperatures, respectively. This formula is due to Bates [152] and has been generalized by Barlow et al. [32] to account for clouds composed of multiple ionic species. The treatment of Barlow et al. also

remains valid even when the $\boldsymbol{E} \times \boldsymbol{B}$ rotation speed of the ion cloud becomes comparable to the ion thermal speed. An important difference between electron and ion charge clouds is evident from Eq. (67). The relaxation rate for electron clouds is much slower and can easily become large compared with the time scale of the experiment. Table 2 provides a useful compendium of some of the transport rates discussed in this section.

Under certain conditions Eq. (67) may fail to properly describe the evolution of a charge cloud's temperature. It is important to realize that the slow expansion caused by ion–neutral mass transport causes heating as ions move down the potential hill created by their own space charge [155]. This effect should only be important for clouds with relatively large central potentials. This heating limits the temperature of electron clouds to 10–50 K even when in contact with a background gas at a temperature of 4 K. A similar effect may elevate the temperature of ion clouds above that of the background neutral gas.

4.3. External transport

All externally induced transport involves some kind of direct interaction between a charge cloud and its external environment. Below we discuss a number of external transport mechanisms that have relevance for FTICR–MS, but it should not be assumed that they form a complete set of possible mechanisms.

The ability to externally control the temperature of a trapped charge cloud has always been one of the most important advantages that these systems offer to both chemical [32] and physical [129] experimentalists. Recorded charge cloud temperatures have spanned almost nine orders of magnitude from 10^{-3} K [129] to 50 eV [156]. Indeed, the upper temperature limit results only from the convenience of using relatively small voltages for trapping. Presumably, a charge cloud inside a toroidal trap [157] could easily be brought to much higher temperatures (although ion–neutral collisions are enhanced for $T > 10$ eV).

The simplest way to heat a trapped charge cloud is to force it to fall down into a potential well, receiving energy directly from electric fields as it does so. Fig. 17 shows a time-sequence of the trapping potentials needed for this process. Shortly after the charge reaches the area of lower

Table 2
Compendium of important transport rates

Internal transport		
Local Maxwellianization ($T_\parallel$ or $T_\perp$)		ν_{ii}
Global Maxwellianization ($T_\parallel$ or $T_\perp$)	$\upsilon_D \geq \rho_c$	ν_{ii}
	$\lambda_D < \rho_c$	$\nu_{ii}(\lambda_D/\rho_c)^2$
Parallel–perpendicular energy exchange	$\epsilon \geq 1$	ν_{ii}
	$\epsilon \ll 1$	$\nu_{ii} I(\epsilon)$
Instability mass transport		ω_R, ω_D
Radial profile rearrangement	$\lambda_D \leq r_L$	$\frac{3}{8}\left(\frac{\omega_p}{\Omega}\right)^4 \nu_{ii}$
Radial profile rearrangement	$\lambda_D \gg r_L$	$\frac{3}{8}\left(\frac{\lambda_D}{r_L}\right)^2 \left(\frac{\omega_p}{\Omega}\right)^4 \nu_{ii}$
Ion–neutral transport		
Radial expansion		$\left[\frac{2\nu_{in}\omega_R}{\Omega}\left(\frac{\mu_{in}}{m_i}\right)\right]^{-1}$
Thermal relaxation		$\frac{2m_i m_n}{(m_i+m_n)^2}\nu_{in}$

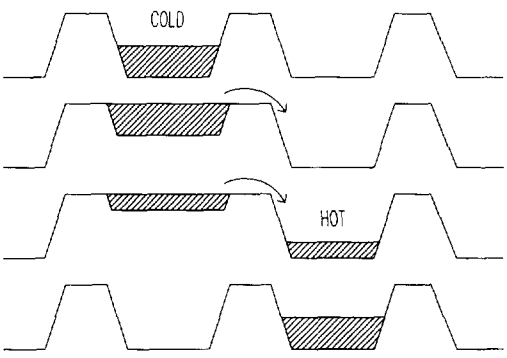

Fig. 17. Time sequence of the necessary trapping potential to achieve "drop" heating. The shaded region represents the trapped charge.

electrical potential energy, collisional processes bring the cloud toward thermal equilibrium, thereby converting its directed kinetic energy into random thermal energy. This process can be repeated to reach any desired temperature. An alternate and somewhat more refined way to heat a trapped charge cloud requires cyclic compression and expansion of the cloud along the magnetic axis [110]. If this motion occurs slowly compared with the ion–ion collision time, the process is adiabatic and little heating occurs. If, however, the process occurs on a timescale comparable with the ion–ion collision time, the cloud's parallel and perpendicular temperatures are unequal during most of the cycle, and heat transfer between these degrees of freedom must result. Fundamental thermodynamics requires that heat flow increases the system's total entropy and therefore results in a net heating over time. This process is often preferred to the simple drop procedure because the heating is more gradual and therefore easier to control. Interestingly, electrical noise of the appropriate frequency can sometimes couple to a trapped charge cloud via the above mechanism, leading to unanticipated and undesired heating.

The existing methods for cooling a trapped ion cloud are far more difficult to implement. Electron clouds cool relatively rapidly via Larmor radiation [114] (gyrating electrons accelerate and radiate their energy), but this process is negligibly slow for ion clouds due to the m^{-3} dependence of the Larmor cooling rate [158]. Laser cooling [159–163] provides a powerful cooling mechanism, but is species-specific and requires a great deal of dedicated apparatus. Sympathetic cooling of one ion species by another may well offer the only general cooling method that can be used for ions of arbitrary mass and charge [164,165]. Sympathetic cooling uses ion–ion collisions to transfer energy between the ions for which cooling is desired and a population of ions for which a viable cooling mechanism exists. For example, a species of negative ions might be cooled by contact with a population of radiatively cooled electrons. Positive ions might be cooled by contact with a population of laser-cooled light ions such as Be^+ [129]. When it is feasible to trap both positively and negatively charged species with dynamic trapping [64], positively charged ions may also be cooled by contact with cold electrons. (However, this coupling is relatively weak.) The time scale for sympathetic cooling is set by the appropriate ion–ion collision rate and by the power of the direct cooling process. Note that ion–neutral collisions may begin to have an important effect on the temperature of cryogenic charge clouds even when they can be ignored for warmer clouds.

Evaporation is an important but often overlooked mechanism for external transport. Under some conditions the most energetic ions within a trapped ion cloud may have sufficient energy to permit their escape over the potential energy barrier at the trap's axial ends. Evaporation is sometimes used deliberately, either to allow the measurement of parallel temperature [45], or to create a more hollow radial density profile by selective evaporation of those ions at the cloud center where the electrical potential is at a maximum [29]. A population of N ions with a Maxwellian distribution of kinetic energies will on average lose

$$N_l = N \exp(-\Delta E/T) \tag{68}$$

ions over a potential energy barrier of height ΔE.

Since a Maxwellian distribution reforms after approximately one ion–ion collision time τ_{ii}, the total fraction of ions lost after a time τ should be

$$f \approx (\tau/\tau_{ii})(N_l/N) \tag{69}$$

Solving for the permissible energy barrier height in terms of the allowable loss fraction f gives

$$\frac{\Delta E}{T} \approx \ln\left(\frac{\tau}{\tau_{ii}} f^{-1}\right) \tag{70}$$

In a typical application one might have $\tau_{ii} = 10^{-3}$ s, $\tau = 10$ s, and $f = 0.01$. Under these conditions, the energy barrier must be at least 14 times the average ion kinetic energy to ensure that less than 1% of the population is lost in 10 s.

The surprisingly large height of the required barrier leads to the conclusion that evaporative loss may be important in FTICR–MS where the charge cloud acquires a tremendous amount of kinetic energy during excitation. The conversion of even a small amount of this coherent kinetic energy into thermal motion may lead to substantial loss of ions out of the axial ends of the trap. Several characteristics of evaporative ion loss may be important for real applications. Because evaporative loss depends strongly on the barrier height, ΔE, loss will not occur uniformly within a particular charge cloud. The trapping and cloud potentials often vary in such a way that hollowing occurs, which can cause rapid mass transport via the diocotron instability [166]. Like ordinary evaporation, axial ion evaporation causes a net cooling, which in turn may effectively limit the total number of ions lost.

As discussed in Section 2, the angular momentum of a charge cloud in a perfectly symmetric trap must be conserved. The gradual radial expansion and eventual charge loss that occur in existing traps must, therefore, arise from the asymmetries or imperfections that are unavoidably present in all real devices [60,104]. Although external mass transport has been thoroughly characterized for a number of devices, a theoretical understanding of the coupling between a trapped charge cloud and the external trapping field errors remains lacking. The discussion that follows describes several external interactions and their effects, but in no case attempts to offer a satisfactory mechanism.

An understanding of the cloud expansion rate due to external transport is important to FTICR–MS for several reasons. Some processes such as ion–molecule reactions and metastable decay may occur over a period of many minutes [167–169]. It is highly desirable that the cloud's shape and size (and temperature) remain constant during this time. In non-neutral plasma physics it has been found that allowing sufficient time after formation for a cloud to approach thermal equilibrium greatly improves experimental reproducibility. In FTICR–MS, however, the utility of this step may be lost if an appreciable cloud expansion occurs during this time. Finally, the length of time that coherent cyclotron motion persists after excitation may depend on the cloud's expansion rate [19]. After the cloud reaches a critical size, external shears or internal stresses may tear it apart, causing it to spread out into an azimuthal ring.

Depending on the neutral gas background pressure, either ion–neutral transport or external transport arising from slight trapping field errors may be the actual cause of external mass transport. An inverse relationship between neutral background gas pressure and charge cloud lifetime τ_m (defined as the time required for the cloud's central density to decrease by half) has been experimentally established for higher pressures [155] ($P > 10^{-7}$ Torr). In this regime, therefore, we expect that ion–neutral transport is of primary importance. As the background gas pressure is decreased, however, the confinement lifetime eventually stops improving. In this regime external transport is the dominant cause of the cloud's radial expansion. A number of different traps all exhibit a lifetime scaling at low pressure that roughly follows the relation [60]

$$\tau_m \propto (B/z_c)^2 \tag{71}$$

where the constant of proportionality is device dependent. There is no accepted explanation for this simple relation, although it is generally agreed that it does not lend any support to the resonant particle transport theories that have been successful in other areas of plasma physics. Fig. 18 shows lifetimes measured by Driscoll et al. [60] from two different traps that follow the scaling given in Eq. (71). Although the dependence of cloud lifetime on parameters other than length and magnetic field is substantially less certain, expansion and loss generally appear to be fastest for dense, narrow clouds. There is little or no agreement about the effect of cloud temperature.

A number of efforts have been made to understand external mass transport by deliberately introducing artificial but well characterized trapping field errors [43]. In every case the connection between asymmetries and transport was established, but simple scaling laws such as Eq. (71) are elusive. Eggleston reports [170] that a specially chosen set of applied asymmetries can even improve the confinement lifetime by up to 40%. It is possible that the applied asymmetries manage to partially cancel the asymmetries naturally present in this device. Notte and Fajans exhaustively investigated the external transport resulting from azimuthal asymmetries of the type that alter the cloud shape as shown in Fig. 10 [171]. Fig. 19 shows the cloud's confinement lifetime versus the perturbing asymmetric voltage that is applied to a single wall patch. Although caution must be exercised in the general application of these results, several interesting conclusions are contained in this work. First, the degradation of confinement lifetime is surprisingly mild, suggesting that an energy conservation law in addition to an angular momentum conservation law may constrain cloud evolution [104]. Second, when an applied asymmetry is sufficiently large that the trap's inherent asymmetries can be ignored, the confinement lifetime scales as

$$\tau_m \propto V_p^{-2} \tag{72}$$

where V_p is the asymmetric voltage applied to a wall patch. Finally, asymmetries add in quadrature, i.e. the confinement lifetime scales as $\tau_m \propto (V_{p1}^2+V_{p2}^2)^{-1}$ when asymmetric voltages V_{p1} and V_{p2} are applied to two separate wall patches.

A final note concerns the difference between the electron clouds used in the non-neutral plasma physics community to study external transport and the ion clouds used in FTICR–MS. Since the traps used in FTICR–MS generally have a strong magnetic field and very short length, Eq. (71) predicts that the confinement lifetime should be very long. However, since the physics that underlies Eq. (71) remains unknown, its applicability to ion clouds is

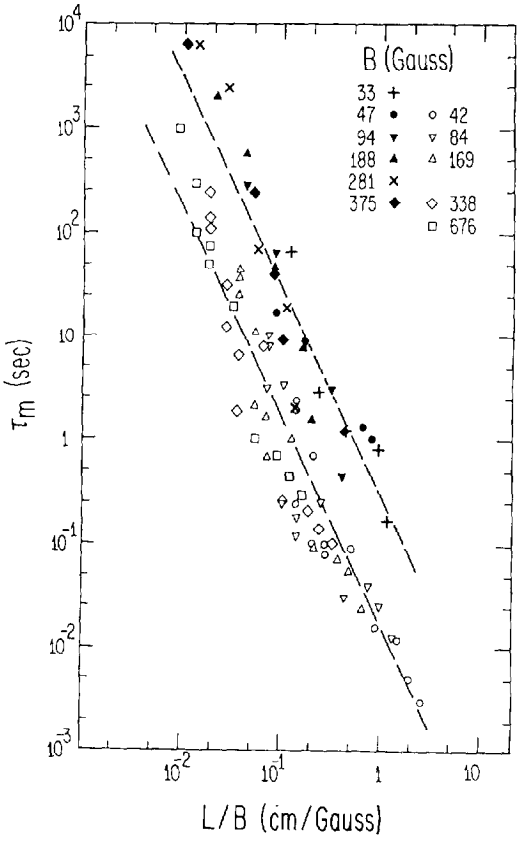

Fig. 18. Data from Driscoll et al. [60] showing measured expansion timescale τ_m versus the ratio; of length L (our z_c) to magnetic field B for two different traps (solid and hollow symbols). The best fit to the data for each trap is shown as a dashed line.

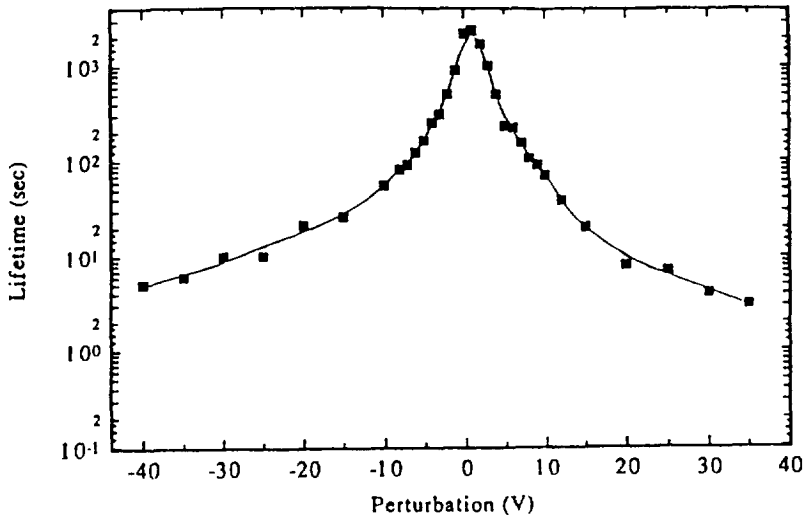

Fig. 19. Data from Notte and Fajans [171] showing cloud confinement lifetime vs. perturbing asymmetric voltage applied to a wall patch.

uncertain. For example, magnetron motion is of great importance for FTICR–MS yet is generally unimportant for electron clouds. The bounce and self-rotation frequencies ω_b and ω_R are comparable for electron clouds but can be very different for ion clouds. Finally, the much more massive ions used in FTICR–MS have larger thermal gyration radii and may therefore undergo more rapid external transport.

5. Modes of oscillation

A salient feature of all ionized systems is that a bewildering variety of oscillatory modes are possible [172]. This final section discusses a number of different modes that have been studied using a non-neutral plasma that have a proven or possible utility for FTICR mass spectrometry. The importance of the cyclotron mode for mass spectrometry needs no discussion. The usefulness of other modes such as the magnetron mode, axial mode, and breathing mode, however, is only beginning to be fully realized. Much of the information that is gathered concerning the state of a trapped charge cloud comes indirectly in the form of mode frequencies, both real and imaginary. The rich mode structure present in these systems affords the experimentalist the opportunity to probe a cloud without necessarily destroying it. Various modes have been used to determine a cloud's composition, temperature, density, radius, or shape.

The first three modes discussed in this section are inherently more fundamental than the others. The slow drift, cyclotron resonance, and axial modes each correspond to one of the possible motions of a single, featureless ion. The other modes discussed below are general, electrostatic modes that involve more complicated patterns of motion among a cloud's ions. Often, these modes do not even take the form of rigid-body motion. Although ion–ion collisions (friction) damp such modes, the damping rate is often sufficiently weak that these modes persist for a time that is long compared with the period of oscillation. Many of these modes are especially useful as diagnostic probes because they are almost completely non-intrusive, producing only a slight increase in the cloud temperature. An electrostatic mode is categorized as a plasma mode or a cyclotron mode depending on whether the relatively rapid cyclotron motion is a necessary part of this mode. Examples of modes from both categories are discussed below.

5.1. Slow drift mode

Certainly, the slow drift mode has the longest history and widest recognition within the physics community [173,174]. A cloud undergoing this mode $\boldsymbol{E} \times \boldsymbol{B}$ drifts around the trap's central axis as a rigid body. Although this mode is called the diocotron or magnetron mode depending on whether space charge or trapping fields cause the drift, any real charge cloud drifts as a result of both causes. Traditionally, plasma physicists work with high density clouds and prefer the name, diocotron, while mass spectrometrists work with relatively low density clouds and prefer the name magnetron. We refer to this mode as the slow drift mode in order to capture its essential physics and avoid the need to choose an existing name that applies only in either the low or high cloud density limits. It is important to contrast the slow drift mode with the drift-like rotational motion that charge clouds normally undergo. Although both the slow drift mode and the drift rotation are the result of $\boldsymbol{E} \times \boldsymbol{B}$ drift, only the slow drift mode is subject to growth, decay, and the other phenomena discussed below.

As expected, the slow drift mode frequency ω_s is identical to the frequency for slow drift ion motion given in Eq. (21). Note that normally other forces such as inertial forces and pressure forces can be neglected, allowing us to write

$$\omega_s \approx \omega_M + \omega_D \tag{73}$$

where ω_M and ω_D are the magnetron and diocotron frequencies defined in Table 1. Eqn (73) appears simple but must be carefully applied to several relevant limiting cases. In FTICR–MS, a charge cloud normally contains sufficiently little space charge that $\omega_M \gg \omega_D$. If possible, however, a measurement of$\omega_D \sim \omega_s - \omega_M$ provides a means to estimate a cloud's total charge. In non-neutral plasma physics, clouds usually contain a large amount of space charge so that $\omega_D \gg \omega_M$ can be assumed. Experiments routinely use ω_s as a simple and direct measure of the linear charge density λ inside the trap [2].

An interesting behavior is predicted by Eq. (73) for clouds with insufficient charge to be considered plasmas or at the axial edge of finite-length clouds that are true plasmas. In either case, ions in the cloud are able to reach a region where the radial electric field exhibits a significant dependence on the axial coordinate z [156]. Because ions with different axial kinetic energies have differing axial motions, they experience different time-averaged radial electric field strengths. It follows that an ion's azimuthal drift speed in such a trap must depend on its axial energy. Fig. 20 shows an experimental verification of this prediction using electron clouds with different monoenergetic axial energies. This effective dependence of magnetron frequency on axial energy may cause the slow drift mode to become unstable in some situations. Fig. 21 contains experimentally obtained images showing the breakup of the slow drift mode. It can be experimentally shown [156] that as this breakup occurs the cloud stretches and separates according to axial energy, i.e. that hot particles move to the cloud's leading edge and cold particles move into the tail. Observation of this breakup of the slow drift mode demonstrates the importance of accounting for both magnetron and diocotron motion in any analysis of the slow drift mode.

The slow drift mode is a negative energy mode because growth of this mode releases electrostatic energy. As a result, a number of mechanisms that can transfer both energy and angular momentum from the cloud to the outside world cause slow drift mode growth. Examples of such processes are ion–neutral collisions [113,175], interaction with an external resistor [18,94], or interaction with transient ions of the opposite charge [142]. Using active circuit elements, it is also possible to create an effectively negative resistance in an external circuit with which a charge cloud interacts. In practice, this feedback is accomplished via the amplification, phase-shifting, and re-application of the signal normally detected in FTICR–MS [94]. Since energy is transferred directly from the charge cloud to the

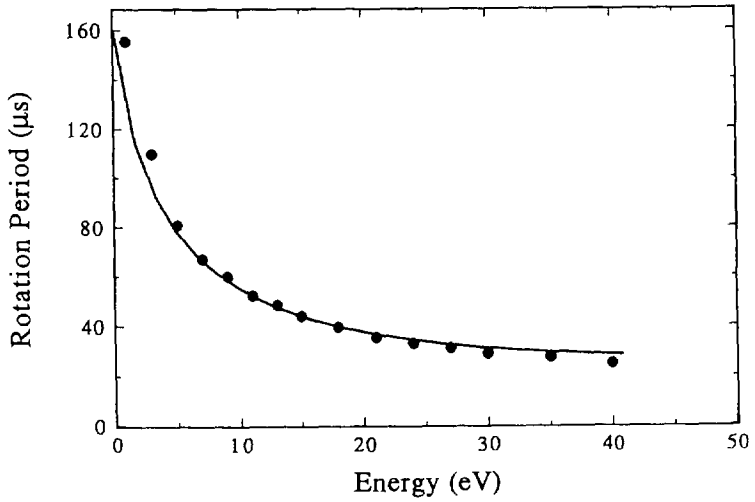

Fig. 20. Measured (points) vs. predicted (smooth curve) azimuthal drift period vs. monoenergetic axial energy for an electron cloud inside the U.C. Berkeley Penning Trap [156].

external circuit, this feedback allows the damping of the slow-drift mode without the necessity of ion–neutral collisions [176]. This technique would be important for any Penning traps designed to operate at very low background neutral gas pressure. The sideband cooling methods currently used in FTICR–MS [143–146], however, depend critically on stochastic ion neutral collisions for ion axialization.

Although the primary effect of a misalignment between a trap's mechanical and magnetic axes is a reduction of the cloud's confinement lifetime, use of the measured lifetime to optimize trap alignment is a difficult and tedious process. It is desirable to have a technique that permits alignment based on information that can be rapidly acquired. Careful observation of the axial distribution of charge in a cloud undergoing the slow drift mode allows such a technique to be implemented [43]. Fig. 22 shows the method used for this technique. If the trap were perfectly aligned, the axial distribution of charge would be time independent. In a misaligned trap, however, whichever end of the charge cloud is closest to the trap wall contains a disproportionate share of the cloud's charge because it is at a lower electrical potential energy. As a misaligned cloud slowly drifts around the trap's central axis, its charge sloshes from end to end. A successful zeroing of the magnitude of this signal is equivalent to an optimization of the trap's alignment.

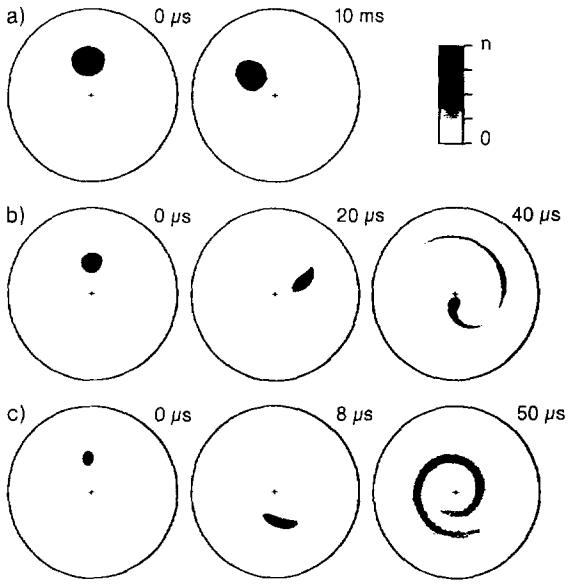

Fig. 21. Time-sequential images showing the evolution of three different electron clouds in the U.C. Berkeley Penning Trap [156]. Cloud (a) is effectively stable while clouds (b) and (c) are increasingly unstable against breakup of the slow drift mode caused by axial energy-dependent "magnetron" drift. The maximum densities for the three sets of images are $n = 2.9 \times 10^7$, 1.7×10^7, and 2.0×10^6, respectively.

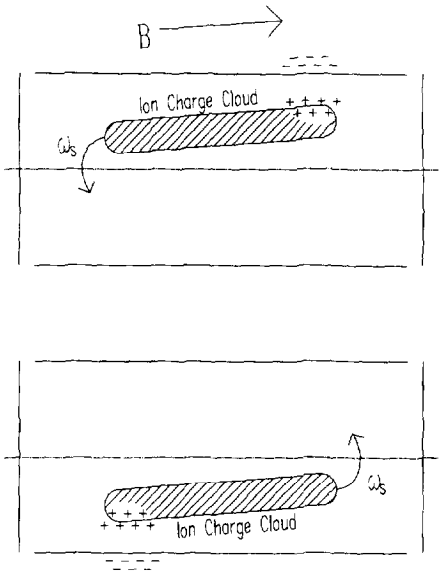

Fig. 22. Diagram illustrating the alignment technique developed by Hart [43]. Charge oscillates axially as the slow drift mode causes first one end, and subsequently the opposite end of a trapped charge cloud to become closest to the trap wall.

5.2. Cyclotron resonance mode

As stated in Section 1, use of the cyclotron resonance mode is far more prevalent in FTICR–MS than in non-neutral plasma physics. Nevertheless, some theoretical work and a limited amount of experimental work have significant application to cyclotron resonance mass spectrometers. The exact frequency of the cyclotron resonance mode given in Section 2 is $\omega_{ICR} = \Omega - \omega_s$, but can be approximated as $\omega_{ICR} \approx \Omega = |q|B/m$ for the purposes of this section. Although we ignore it here, it is important to note that the frequency of the cyclotron resonance mode depends directly on the frequency of the slow drift mode and it is therefore subject to many of the effects discussed in the preceding subsection.

Like slow drift motion, cyclotron motion can take the form of rotation about the cloud's central axis or gyration of the entire cloud within the trap. While the latter motion at $\Omega - \omega_s$ is the ion cyclotron resonance mode exploited for FTICR–MS, the former motion occurs at $\Omega - \omega_R$ and has received comparatively little attention. This cyclotron-like rotation is not strictly a mode because it is merely one of two possible rotational states available to the charge cloud; it is not subject to growth and decay. A cloud that undergoes this cyclotron-like rotation is experimentally quite difficult to obtain. One possible method is the addition of a large amount of angular momentum via torque from a laser beam as shown in Fig. 8 [76]. Alternately, a charge cloud enters the fast rotational mode if it is rapidly passed through a magnetic cusp [84] (a region of space where the magnetic field reverses its axial direction). Caution must be exercised within the non-neutral plasma literature where the phrase cyclotron mode refers to either the cyclotron resonance mode, the cyclotron-like rotational state, or even the additional cyclotron modes discussed briefly below.

Both the slow drift mode and the cyclotron mode can be arbitrarily combined with the two available rotational states, leading to the possible creation of charge clouds in exotic and potentially useful dynamical states. For example, a cloud may be excited into either the slow drift or cyclotron resonance modes while undergoing cyclotron-like rotation. The experimental properties of such clouds are as yet unexplored.

Under the conditions normally used in FTICR–MS, the coherent gyration of a cloud in the cyclotron resonance mode is extraordinarily stable. It can be shown that stability is enhanced for dense, cold, and narrow clouds confined in traps with approximately harmonic potential wells [19]. Under some conditions cloud expansion may cause the cloud to tear apart and smear into an azimuthal ring. Surprisingly, it has been theoretically calculated that such a ring is not susceptible to the diocotron instability that affects drifting azimuthal rings [83]. The cyclotron resonance coherence time for multiple charge clouds may also be limited by transport caused by cloud–cloud collisions. The collisions between ions in separate clouds are one possible mechanism for this transport. It appears, how-

ever, that the limitations imposed by this type of transport can be ignored for the current generation of FTICR–MS ion traps. Even for a single charge cloud, energy is removed from the cyclotron resonance mode by ion–neutral collisions. Because this mode has positive energy (in contrast to the slow drift mode), energy removal causes the mode amplitude to decrease.

The Coulombic interaction between multiple charge clouds undergoing the cyclotron resonance mode greatly complicates their dynamics. Even for two charge clouds there is a substantial range of possible behaviors. Clouds containing ions with very similar q/m ratios may phase-lock, causing a failure of the mass spectrometer to resolve these two ions [177]. Clouds containing ions with roughly equal q/m ratios experience a modulation from the periodic gradual collisions that these clouds undergo [17]. Clouds containing ions with substantially different q/m ratios interact in one of two ways depending on whether their cyclotron resonance frequencies ω_{ICR1} and ω_{ICR2} are commensurate ($\omega_{ICR1}/\omega_{ICR2}$ takes the form of a ratio of integers) [178]. Gyrators with incommensurate frequencies experience a frequency shift that depends on the amount of space-charge present in each cloud and the relative difference in their gyration radii. This frequency shift has been experimentally observed by Gorshkov et al. [16]. Gyrating clouds with commensurate frequencies, however, may experience more severe space-charge effects as they exchange energy and angular momentum over a relatively long time scale. This behavior occurs for commensurate gyrators because their collisions always occur at the same azimuthal location within the trap. Note that the occurrence of commensurate gyrators is not uncommon in FTICR–MS because of the constancy of the electron's charge and because masses tend to differ by nearly exact multiples of the atomic mass unit. Numerical simulations indicate that three or more interacting commensurate gyrating clouds often behave chaotically, leading to unpredictable and irreproducible dynamics. Fig. 23 shows the gyration radii of three such clouds as a function of time. Should this behavior occur in actual experiments, one would expect a substantial broadening of the peaks in a mass spectrum. The severity of these space-charge effects is conveniently parametrized by the dimensionless number $mN/4\pi\epsilon_0 r_c^3 B^2$, where N is the number of ions assumed to be in each cloud and r_c is the radius of the cyclotron resonance mode. Note that space-charge effects are minimized at high magnetic field and for low mass ions at large cyclotron mode amplitudes.

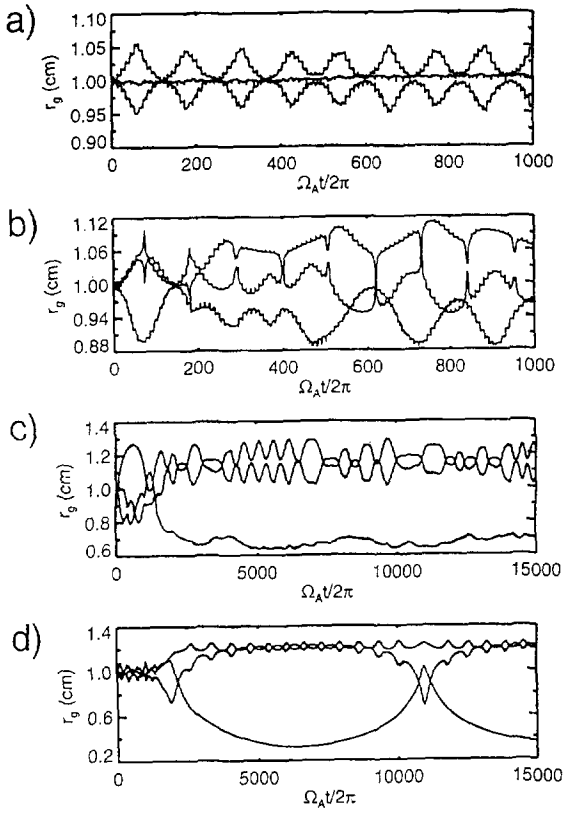

Fig. 23. Numerically calculated data from Peurrung and Kouzes [178] showing gyration radii of three commensurate ion clouds vs. number of gyration orbits for ion cloud A ($\Omega_A t/2\pi$). These plots show examples of the chaotic or unusual dynamics that can occur for three interacting ion clouds. All clouds start 120° apart with r_g = 1.0 cm in a trap with B = 3T and contain ions with Z = 6e. The ion masses are 9 000 u, 10 000 u, and 8 050 u (a), 9 900 u (b), 8 183 u (c), or 8 999 u (d). The number of ions per cloud is 3 000 (a), 3 000 (b), 2 000 (c), and 1 500 (d).

5.3. Axial mode

The axial mode of oscillation at the frequency ω_z has long been one of the most important tools for the study of single trapped particles [4,179]. This mode has received comparatively less attention, however, for entire charge clouds [32,176,180]. A primary reason for this relative neglect is related to the restricted conditions under which this mode is highly stable. Only clouds composed of ions with a single charge-to-mass ratio in perfectly harmonic axial potential wells undergo long-term coherent axial motion. The fragility of this mode arises from the fact that there is no stabilizing effect to preserve mode coherence in the presence of non-ideal conditions. The slow drift and cyclotron resonance modes, in contrast, are both stabilized by the averaging effect of the cloud's inevitable rotation. (The success of FTICR–MS is attributable to this stabilizing effect [19].) Any effect that changes the environment of a charge cloud as it oscillates axially causes the cloud to slowly heat and expand, ultimately destroying the coherence of the mode. For example, the curvature of a non-harmonic potential well depends on z, causing the shape of a charge cloud to change as it undergoes axial oscillations. This shape change in turn launches internal modes that convert coherent kinetic energy into random thermal energy as they decay. In addition, a cloud containing multiple species of ions must fragment into single-species clouds upon excitation of the axial mode. The subsequent collisions of these clouds leads to mode degradation on a timescale associated with the frequency for collisions between ions from separate clouds.

Despite the fragility of the axial mode, it has been used with great success for a variety of diagnostic applications. A significant advantage of the axial mode is that both excitation and detection can be accomplished without the need for azimuthally segmented electrodes. A technique known as Fourier transform ion z resonance mass spectrometry (FTIZR–MS) provides an alternate means to obtain the mass spectrum of a trapped ion cloud [181]. This technique functions quite similarly to FTICR–MS except that the axial mode instead of the cyclotron resonance mode is excited and detected. In contrast to FTICR–MS, the mode's decay rate provides additional diagnostic information on the ion–ion collision frequency [32,180].

Another useful diagnostic technique deserves mention despite the fact that it utilizes the incoherent axial oscillation of cloud ions rather than the coherent axial mode. Direct, non-intrusive ion calorimetry exploits the fact that the energy absorbed by a charge cloud during an excitation of fixed amplitude, frequency, and duration depends directly on the number of resonant cloud ions. A mass spectrum is acquired by monitoring the axial temperature with one of the trap's two endcaps while the frequency of an excitation signal applied to the other endcap is slowly varied. The frequencies at which temperature rises are detected indicate specific species present inside the cloud, and the amount of temperature rise indicates the amount of that species that is present. The excitation signal used for this calorimetric technique could be any signal with a response among the cloud ions that depends in some known way on ion mass. Current implementations of this technique [32,181–184] utilize the breathing mode because of its ease of use and because its relatively high frequency permits high mass sensitivity. Although spectra acquired in this way have a quality that is clearly inferior to FTICR–MS spectra, there is the advantage that the cloud remains cold and quiescent at all times, never undergoing violent collisions with neutral species.

5.4. Mode conversion

For each pair of the three above modes there is an appropriate electrical signal that accomplishes a complete exchange of magnitude and phase between the two modes. Such interconversions have found a rapidly growing application in

FTICR–MS and represent a hugely successful borrowing of technology from the physics trapping community [4,185,186] to the area of mass spectrometry [143–146]. Common to all of the existing applications is an exploitation of some significant difference between the properties of the three basic modes.

One of the primary applications for these techniques is cloud compression. Because the slow drift (magnetron) mode is a negative energy mode, a variety of processes tend to increase the mode amplitude. Increased magnetron mode amplitude can be manifested in either of two ways. Coherent magnetron mode growth causes the entire cloud to spiral radially outward as it slowly orbits the trap's central axis. Incoherent mode growth causes the entire cloud to expand radially while remaining centered. Specific causes of cloud expansion could be any of the violent processes to which an ion cloud is subjected such as ion–neutral collisions [146] or cyclotron resonance excitation. It is difficult to remeasure the mass spectrum of an expanded cloud since it is less stable in the cyclotron mode. (Such a cloud rotates less quickly about its own central axis samples a greater region of spatial inhomogeneity.) Cloud compression requires the complete exchange of magnetron mode energy with that of either the axial or cyclotron modes. Immediately after such an exchange the cloud would be neither more compact nor more centered. However, subsequent rapid damping of cyclotron or axial mode energy via ion–neutral collisions leaves the cloud in a highly compact, centered state that is ideal for remeasurement with FTICR mass spectrometry.

Interconversion also finds application in the area of cloud cooling. This technique exploits the fact that it is often easier to cool one of the three basic modes than the other two. For example, suppose that the axial motion can be rapidly cooled by interaction with an external circuit containing a cryogenically cooled resistor. In this case drift-axial and cyclotron-axial interconversions permit the total cooling of the trapped cloud with a single cooling mechanism [176].

The final application for interconversion exploits the relative slowness of magnetron motion. Because the magnetron motion is relatively slow, it is possible to perform detailed manipulation of the amplitude and phase of clouds in the slow drift mode. Subsequent interconversion transfer this controlled arrangement to the cyclotron mode while the existing cyclotron amplitude and phase enter the magnetron mode. This technique thus provides the ability to control the phase and amplitude of multiple charge clouds in the cyclotron resonance mode, making possible a number of interesting experiments. For example, Chen et al. [89,187] have demonstrated the possibility of detection at the harmonic frequency $2\omega_{ICR}$ using two identical charge clouds that are 180° apart in orbital phase. In addition, careful control over the amplitude of cyclotron motion may provide a route toward investigation or elimination of space-charge effects.

5.5. Additional electrostatic modes

Electrostatic modes occur in a variety of forms depending on the cloud shape, size, and type of excitation. In this section we restrict our discussion to those modes that have either found a demonstrated diagnostic application or could conceivably do so without great effort. A classification based on frequency provides a useful conceptual means of separating modes into logical groupings. The two groups discussed below have frequencies that are loosely grouped around the cyclotron frequency (cyclotron modes) Ω, and the plasma frequency ω_p (plasma modes).

Recent theoretical and experimental work has shown that the axial, slow drift, and cyclotron resonance modes are in fact merely a low-order subset of a much broader class of electrostatic modes. This infinite set of modes are simply the possible normal modes of oscillation of a cold, spheroidal charge cloud under the assumption

that it can be treated with conventional fluid theory of plasma dynamics [188]. (This excludes many of the cyclotron modes discussed above.) A general treatment of this set of modes, which include both fast (Ω) and slow (ω_s) modes is available in the literature [85,121,189] and is not discussed further here.

5.5.1. Cyclotron modes

A cyclotron mode consists of any organized (i.e. not random or thermal) pattern of cyclotron motion among the individual ions making up a particular cloud. Fig. 24 shows three of the simplest possible cyclotron modes discussed below. The normal modes for many dynamical systems are often conveniently labeled with a set of indices. For example, the modes of oscillation for a circular drumhead require two quantized mode numbers and the hydrogen atom requires three. For a number of simple examples of cyclotron mode phenomena, the mode amplitude can be written

$$\phi(r,\theta,z) = Af(r)e^{ik_z z}e^{im\theta} \tag{74}$$

where $f(r)$ describes the mode amplitude's radial variation, m is the quantized azimuthal mode number, and k_z is the mode's axial wave number. (Eq. (74) cannot be used for cyclotron mode phenomena generally.) All of the cyclotron modes investigated to date have had $k_z = 0$. (Considering the rapid axial transport in such systems, $k_z \neq 0$ may not be feasible.) The special case for which $f(r) = 1$ and $m = 1$ is the familiar cyclotron resonance mode used in FTICR–MS.

One particular mode known as the breathing mode (Fig. 24(a)) has received particular attention [32,183,184] as a diagnostic tool. This mode has the characteristics $m = 0$, $f(r) \sim r$ and a mode frequency that is precisely equal to the vortex frequency $\omega_V = \Omega - 2\omega_R$. This mode is of primary use in axially short traps since this mode's perfect azimuthal symmetry requires excitation and detection with the use of the trap's endcaps. An application for the breathing mode involves the use of ion cloud calorimetry as described above in connection with the axial mode. The mode amplitude, which again indicates the number of resonant cloud ions, is measured as the cloud's axial temperature after sufficient time has elapsed for mode decay. This method of acquiring a mass spectrum is quite gentle, and the relatively large frequencies involved permit an accurate mass measurement. Barlow et al. [32] have successfully acquired mass spectra with a resolution of 10^4 using this method. Fig. 25 contains an example of such a mass spectrum. A further possible advantage of this technique is that the mode is excited by a simple modulation of the trapping potential. This allows the construction of a trap without a ring electrode that is divided into azimuthal sectors and the

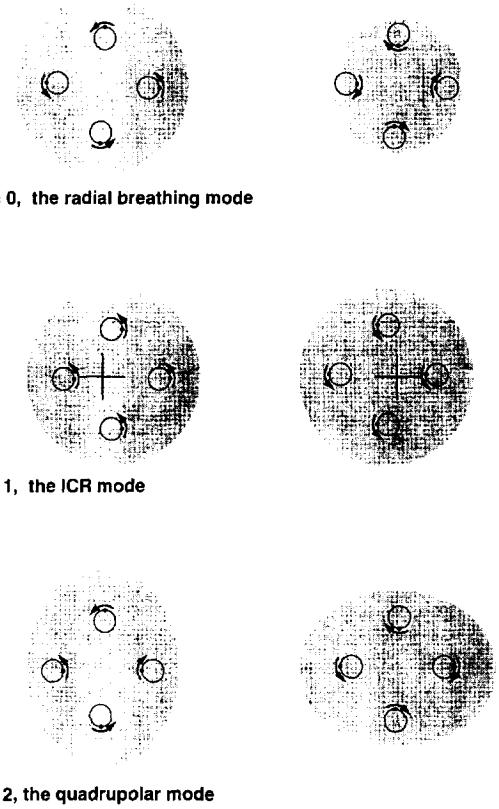

Fig. 24. Two examples of cyclotron modes that do not involve rigid, center-of-mass motion of the charge cloud. As discussed in the text, the "breathing" mode shown in (a) occurs at the vortex frequency ω_V, while the "internal dipole" mode shown in (b) occurs at the cyclotron resonance frequency ω_{ICR}.

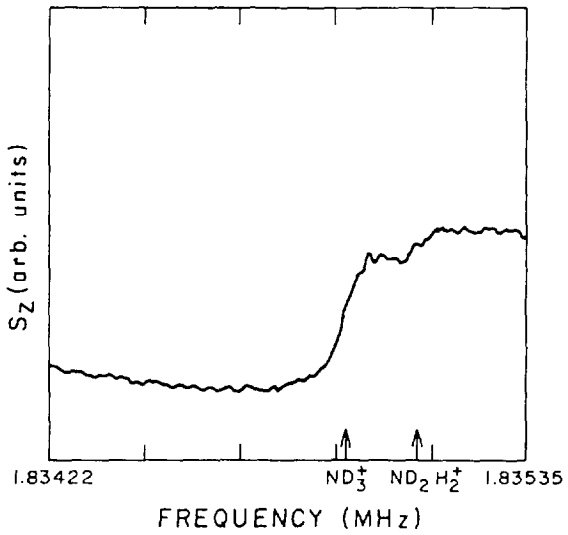

Fig. 25. High resolution mass spectrum of an ion sample taken from Barlow et al. [32]. Shown is a trace of noise power versus applied cyclotron heating frequency. The larger rise at lower frequency is due to ND_3^+ and the smaller rise is due to $ND_2H_2^+$, but with about 10 times greater sensitivity due to increased heating. The mass resolution is greater than 10 000.

accompanying excitation and detection non-idealities.

A number of additional cyclotron modes have been studied [42,86,87], including modes with m = 1,2,3, and 4, and a variety of radial mode profiles $f(r)$. The frequencies of these modes contain information about the cloud's central rotation rate ω_R (in this experiment the cloud is not a rigid-rotor), the ratio r_L/ρ_c of the thermal Larmor gyration radius to the cloud size, and the radial density profile. The $m = 1$ mode studied by Gould (Fig. 24(b)) is physically similar to the cyclotron resonance mode used in FTICR–MS. Both modes have the frequency $\omega_{ICR} = \Omega - \omega_s$ and involve a new motion of the cloud's center of mass. The essential difference between the non-neutral plasma and FTICR–MS versions of this mode is that Gould studied large clouds undergoing small-amplitude motion, while FTICR–MS utilizes the large-amplitude motion of small clouds.

5.5.2. *Plasma modes*

Several investigations have demonstrated the utility of plasma modes for the determination of a charge cloud's density, shape, size, and temperature [176,190]. Fig. 26 shows a number of the modes that can be used as diagnostic tools. In the first of these studies, Weimer et al. [176] trapped a cloud with aspect ratio $\alpha \ll 1$, i.e. a very axially thin, disk-shaped cloud. In this regime, $\omega_p \sim \omega_z$ and a number of the possible mode frequencies are closely spaced near $\omega = \omega_p$. Measurement of the time dependence of these mode frequencies as shown in Fig. 27 allows direct determination of the plasma's time-dependent aspect ratio. This measured aspect ratio together with the measured axial oscillation frequency ω_z and the total cloud charge determined by other mode diagnostics completely determine the cloud's shape, size, density, and rotation frequency. A similar diagnostic procedure has been utilized by Tinkle et al. [190] for the regime where $\alpha \geq 1$. This work also verifies that mode frequencies exhibit a slight dependence on cloud temperature [189]. As a result, it is possible to determine the cloud temperature in addition to the parameters relating to the cloud's density profile.

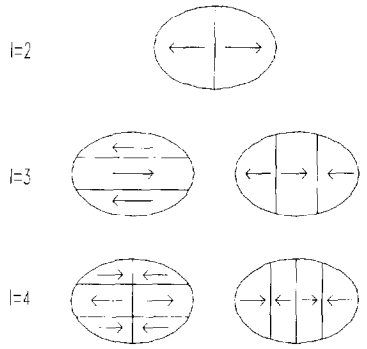

Fig. 26. Sketches showing a number of the electrostatic modes used as diagnostics by Tinkle et al. [190]. These modes are azimuthally symmetric so that only a cross-section of the charge cloud is shown. The index l describes these modes in such a way that l–1 is the number of nodes present as the mode oscillates. Each of these modes causes internal motion as indicated by the arrows. The straight lines within the charge clouds indicate the nodes where no motion occurs.

Clouds trapped in very elongated traps have non-spheroidal (approximately cylindrical, see Section 3) shapes that cannot be easily treated

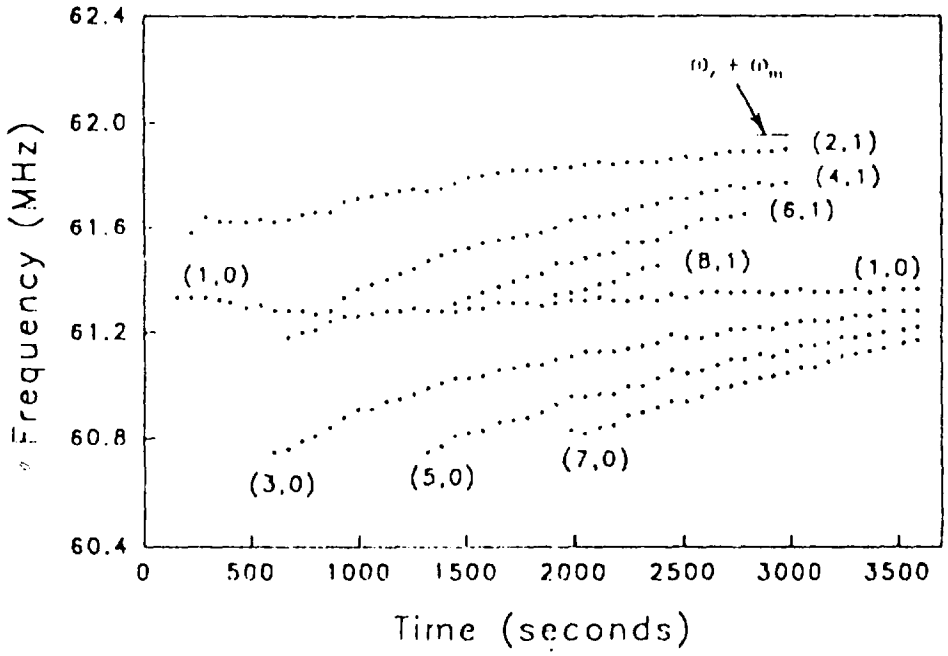

Fig. 27. A plot from Weimer et al. [176] showing the frequencies of the modes vs. time after the cloud was loaded; for all points the measurement uncertainty in the frequency is less than the symbol size used.

by the above normal mode analysis. However, two experiments have shown that the density and temperature of such a charge cloud can easily be determined from a measurement of the dispersion relation for propagating Langmuir waves [39,191]. (A Langmuir wave is a simple electrostatic compressional wave that propagates along the magnetic field. This wave is a logical counterpart to the low-order axial compressional modes used by Tinkle et al. [190].) In summary, any well-characterized measurement of electrostatic mode frequencies for a trapped charge cloud contains sufficient information to completely determine the cloud's thermal equilibrium state.

6. Concluding remarks

The primary purpose of this review is to facilitate communication and collaboration between practitioners of non-neutral plasma physics and FTICR–MS. Traditional barriers between these two groups have included differences in vocabulary, academic background, and area of application. FTICR–MS instruments are now being commercially manufactured and deployed in an increasing variety of settings, while non-neutral plasma physics remains firmly tied to institutions that are strong in theoretical physics. Non-neutral plasma physics and FTICR–MS have independently come to similar conclusions about the Penning trap: non-neutral plasma physicists view it as a powerful experimental tool with a proven ability to perform experiments of unequaled sensitivity, while mass spectroscopists are attracted to its inherent resolution and versatility.

Both FTICR–MS and much of non-neutral plasma physics employ a Penning trap to confine a substantial amount of charge. This similarity provides a powerful connection between these fields despite a number of apparent differences. For example, diocotron drift is of primary importance in non-neutral plasma physics and magnetron drift dominates in FTICR–MS, yet both motions are simply the result of radial electric fields. Non-neutral plasma physicists have extensively studied the slow drift mode

and FTICR–MS has made great use of the ion cyclotron resonance mode, yet these modes are simply related by a straightforward change in the frame of reference. Non-neutral plasma physics has historically utilized only cylindrical traps built with exacting mechanical symmetry and FTICR–MS has utilized a variety of trap designs, yet many trap characteristics are independent of the details of trap design. In contrast, FTICR–MS instruments typically employ high quality NMR magnets, while non-neutral plasma physics experiments commonly employ magnets with lower homogeneity.

The remaining concluding remarks consist of a number of unproved assertions that we feel are useful for applying the literature of non-neutral plasma physics to the problems of FTICR–MS.

The existence of a plasma is not always necessary for the validity of particular results. A remarkable amount of the material that falls within the domain of non-neutral plasma physics can be confidently applied to any trapped charge cloud. This is certainly true when the physics is stated explicitly in terms of the cloud's Debye length.

It is useful to distinguish between those elements of cloud dynamics that depend on a cloud's many-body nature, and those that do not. Often, trap physics can be easily understood as the physics of a single ion. The ion cyclotron resonance mode, for example, is a single-particle motion while effects that impair the stability of this mode may require the action of many different ions within the cloud.

Understanding a cloud's inevitable approach towards a thermal equilibrium state can help solve many experimental problems. A knowledge of non-equilibrium transport allows the estimation of a clouds characteristics at any particular moment in time.

An understanding of ion–neutral interactions and their effects is important for careful interpretation of experimental data. Whether such effects are intended or merely detrimental, they often cannot be ignored.

Results obtained with a particular trap design can often be applied to traps with alternate designs. Most traps are approximately harmonic and the nature of any imperfections is often remarkably unimportant to the basic physics. Additionally, drastically non-harmonic traps may experience the same phenomenon as a nearly harmonic trap, only to a greater degree.

References

[1] C. Roberson and C. Driscoll (eds.), Non-Neutral Plasma Physics, AIP, New York, 1988.
[2] R.C. Davidson, Physics of Nonneutral Plasmas, Addison–Wesley, Redwood City, 1990.
[3] J.B. Jeffries, S.E. Barlow and G.H. Dunn, Int. J. Mass Spectrom. Ion Processes, 54 (1983) 169.
[4] L.S. Brown and G. Gabrielse, Rev. Mod. Phys., 58 (1986) 233.
[5] S.K. Huang, D.L. Rempel and M.L. Gross, Int. J. Mass Spectrom. Ion Processes, 72 (1986) 15.
[6] F.H. Laukien, Int. J. Mass Spectrom. Ion Processes, 73 (1986) 81.
[7] S. Guan and P.R. Jones, J. Chem. Phys., 91 (1989) 5291.
[8] S.E. Delong, D.W. Mitchell, D.J. Cherniak and T.M. Harrison, Int. J. Mass Spectrom. Ion Processes, 91 (1989) 273.
[9] B.A. Hearn, C.H. Watson, G. Baykut and J.R. Eyler, Int. J. Mass Spectrom. Ion Processes, 95 (1990) 299.
[10] M.A. May, P.B. Grosshans and A.G. Marshall, Int. J. Mass Spectrom. Ion Processes, 120 (1992) 193.
[11] C.L. Holliman, D.L. Rempel and M.L. Gross, J. Am. Soc. Mass Spectrom., 3 (1992) 460.
[12] X. Xiang, P.B. Grosshans and A.G. Marshall, Int. J. Mass Spectrom. Ion Processes, 125 (1993) 33.
[13] S.P. Chen and M.B. Comisarow, Rapid Commun. Mass Spectrom., 5 (1991) 450.
[14] E.A. Cornell, K.R. Boyce, D.L.K. Fygenson and D.E. Pritchard, Phys. Rev. A, 45 (1992) 3049.
[15] G.T. Uechi and R.C. Dunbar, J. Am. Soc. Mass Spectrom., 3 (1992) 734.
[16] M.V. Gorshkov, A.G. Marshall and E.N. Nikolaev, J. Am. Soc. Mass Spectrom., 4 (1993) 855.
[17] C.L. Hendrickson, S.C. Beu and D.A. Laude, J. Am. Soc. Mass Spectrom., 4 (1993) 909.
[18] S.C. Beau and D.A. Laude, Int. J. Mass Spectrom. Ion Processes, 108 (1991) 255.
[19] A.J. Peurrung and R.T. Kouzes, Phys. Rev. E, 49 (1994) 4362.
[20] A.W. Hyatt, C.F. Driscoll and J.H. Malmberg, Phys. Rev. Lett., 59 (1987) 2975.
[21] D.L. Eggleston and J.H. Malmberg, Phys. Rev. Lett., 59 (1987) 1675.

[22] E. Okress, Cross-field Microwave Devices, Academic Press, New York, 1961.
[23] J.S. Wurtele, R. Chu and J. Fajans, Phys. Fluids B, 1 (1989) 2073.
[24] C.A. Kapetenakos and P. Sprangle, Phys. Today, 38 (2), (1985) 58.
[25] T.E. Cowan et al., Hyperfine Interactions, 76 (1993) 135.
[26] C.M. Surko, A. Passner, M. Leventhal and F.J. Wysocki, Phys. Rev. Lett., 61 (1988) 1831.
[27] F.C. Michel, Comments on Astrophysics. Comments on Modern Phys. Part C, 13 (1989) 145.
[28] K.S. Fine, C.F. Driscoll, J.H. Malmberg and T.B. Mitchell, Phys. Rev. Lett., 91 (1991) 588.
[29] A.J. Peurrung and J. Fajans, Phys. Fluids A, 5 (1993) 493.
[30] J.J. Bollinger, D.J. Heinzen, W.M. Itano, S.L. Gilbert and D.J. Wineland, Phys. Rev. Lett., 63 (1989) 1031.
[31] S.R. Elliot et al. Hyperfine Interactions, 81 (1993) 151.
[32] S.E. Barlow, J.A. Luine and G.H. Dunn, Int. J. Mass Spectrom. Ion Processes, 74 (1986) 97.
[33] A.G. Marshall and F.R. Verdun, Fourier Transforms in NMR, Optical and Mass Spectrometry, Elsevier, Amsterdam, 1990.
[34] B. Asamoto (ed.), Analytical applications of Fourier transform ion cyclotron resonance mass spectrometry, VCH publishers, New York, 1991.
[35] A.G. Marshall and P.B. Grosshans, Anal. Chem., 63 (1991) 215.
[36] C.C. Wang, Proc. IRE, 38 (1950) 135.
[37] J.C. Helmer and R.L. Jepsen, Proc. IRE, 49 (1961) 1920.
[38] L.D. Hall, Rev. Sci. Instrum., 29 (1958) 367.
[39] J.H. Malmberg and J.S. deGrassie, Phys. Rev. Lett., 35 (1975) 577.
[40] J.D. Daugherty, J.E. Eninger and G.S. Janes, Phys. Fluids, 12 (1969) 2677.
[41] C.A. Kapentanakos, R.E. Pechacek, D.M. Spero and A.W. Trivelpiece, Phys. Fluids, 14 (1971) 1555.
[42] R.W. Gould and M.A. LaPointe, Phys. Rev. Lett., 67 (1991) 3685.
[43] G.W. Hart, Phys. Fluids B, 3 (1991) 2987.
[44] J.D. Moody and J.H. Malmberg, Phys. Rev. Lett., 69 (1992) 3639.
[45] D.L. Eggleston, C.F. Driscoll, B.R. Beck, A.W. Hyatt and T.H. Malmberg, Phys. Fluids B, 4 (1992) 3432.
[46] A.J. Peurrung and J. Fajans, Rev. Sci. Instrum., 64 (1993) 52.
[47] F.F. Chen, Plasma Physics and Controlled Fusion, Plenum Press, New York, 1984, p. 8.
[48] J.H. Malmberg and T.M. O'Neil, Phys. Rev. Lett., 39 (1977) 1333.
[49] D.H.E. Dubin and T.M. O'Neil, Phys. Rev. Lett., 60 (1988) 511.
[50] S.L. Gilbert, J.J. Bollinger and D.J. Wineland, Phys. Rev. Lett., 60 (1988) 2022.
[51] J. Beebe-Wang, N. Elander and R. Schuch, Phys. Scr., 46 (1992) 560.
[52] J.J. Bollinger and D.J. Wineland, Sci. Am., 262 (1990) 124.
[53] F.M. Penning, Physica (Utrecht), 3 (1936) 873.
[54] G. Gabrielse, L. Haarsma and S.L. Rolston, Int. J. Mass Spectrom. Ion Processes, 88 (1989) 319.
[55] J.R. Pierce, Theory and Design of Electron Beams, 2nd Van Nostrand Co., New York, 1954, p. 41.
[56] W.W. Yin, M. Wang, A.G. Marshall and E.B. Ledford, J. Am. Soc. Mass Spectrom., 3 (1992) 188.
[57] R.L. Hunter, M.G. Sherman and R.T. McIver, Int. J. Mass Spectrom. Ion Processes, 50 (1983) 259.
[58] M. Wang and A.G. Marshall, Anal. Chem., 61 (1989) 1288.
[59] J.A. Castoro, C. Koster and C.L. Wilkins, Anal. Chem., 65 (1993) 784.
[60] C.F. Driscoll, K.S. Fine and J.H. Malmberg, Phys. Fluids, 29 (1986) 2015.
[61] M. Wang and A.G. Marshall, Anal. Chem., 62 (1990) 515.
[62] C.D. Hanson, M.E. Castro, E.L. Kerley and D.H. Russell, Anal. Chem., 62 (1990) 520.
[63] P.A. Limbach, P.B. Grosshans and A.G. Marshall, Int. J. Mass Spectrom. Ion Processes, 123 (1993) 41.
[64] M.V. Gorshkov, S. Guan and A.G. Marshall, Rapid Commun. Mass Spectrom., 6 (1992) 166.
[65] D.J. Bate, K. Dholakia, R.C. Thompson and D.C. Wilson, J. Mod. Opt., 39 (1992) 305.
[66] K. Dholakia, G. Zs. K. Horvath, D.M. Segal, R.C. Thompson, D.M. Warrington and D.C. Wilson, Phys. Rev. A, 47 (1993) 441.
[67] G. Gabrielse et al. Phys. Rev. Lett., 65 (1990) 1317.
[68] R.S.V. Dyck, D.L. Farnham and P.B. Schwinberg, Phys. Rev. Lett., 70 (1993) 2888.
[69] C.B. Lebrilla, D.T.S. Wang, R.L. Hunter and R.T. McIver, Anal. Chem., 62 (1990) 878.
[70] S.A. Hofstadler and D.A. Laude, Anal. Chem., 64 (1992) 569.
[71] T. Solouki, K.J. Gillig and D.H. Russel, Anal. Chem., 66 (1994) 1583.
[72] J.E. Bruce et al. J. Am. Chem. Soc., 116 (1994) 7839.
[73] R.D. Smith, Nature, 369 (1994) 137.
[74] R. Chen, Q. Wu, D.W. Mitchel, S.A. Hofstadler, A.L. Rockwood and R.D. Smith, Anal. Chem., 66 (1994) 3964.
[75] R. Chen et al., Anal. Chem., (1995) in press.
[76] D.J. Heinzen, J.J. Bollinger, F.L. Moore, W.M. Itano and D.J. Wineland, Phys. Rev. Lett., 66 (1991) 2080.
[77] C.M. Surko and T.J. Murphy, Phys. Fluids B, 2 (1990) 1372.
[78] L.H. Haarsma, K. Abdullah and G. Gabrielse, Phys. Rev. Lett., 75 (1995) 806.
[79] W.R. Crea and J.T. Brenna, Chem. Phys., 126 (1988) 453.
[80] G.H. Kruppa et al., in B. Asamoto (ed.), FT–ICR/MS: Analytical Applications of Fourier Transform Ion Cyclotron Resonance Mass Spectrometry, VCH Publishers, New York, 1991, p. 107.
[81] B.E. Winger, S.A. Hofstadler, J.E. Bruce, H.R. Udseth and R.D. Smith, J. Am. Soc. Mass Spectrom., 4 (1993) 566.
[82] H. von Koding, F.A. Pinkse and N.M.M. Nibbering, Rapid Commun. Mass Spectrom., 7 (1993) 780.
[83] A. Nocentini, H.L. Berk and R.N. Sudan, J. Plasma Phys., 2 (1968) 311.
[84] A.J. Theiss, R.A. Mahaffey and A.W. Trivelpiece, Phys. Rev. Lett., 35 (1975) 1436.
[85] J.J. Bollinger, D.J. Heinzen, F.L. Moore, W.M. Itano, D.J. Wineland and D.H.E. Dubin, Phys. Rev. A, 48 (1993) 525.

[86] R.W. Gould and M.A. LaPointe, Phys. Fluids B, 4 (1992) 2038.
[87] R.G. Greaves, M.D. Tinkle and C.M. Surko, Phys. Rev. Lett., 74 (1995) 90.
[88] C.L. Hendrickson, S.A. Hofstadler, S.C. Beu and D.A. Laude, Int. J. Mass Spectrom. Ion Processes, 123 (1993) 49.
[89] R.D. Chen, S.H. Guan and A.G. Marshall, J. Chem. Phys., 100 (1994) 2258.
[90] L. Brillouin, Phys. Rev., 67 (1945) 260.
[91] A.J. Peurrung and J. Fajans, Phys. Fluids B, 2 (1990) 693.
[92] M.V. Gorshkov and E.N. Nikolaev, Int. J. Mass Spectrom. Ion Processes, 125 (1993) 1.
[93] R.S. VanDyck, R.L. Moore, D.L. Farnham and P.B. Schwinberg, Phys. Rev. A, 40 (1989) 6308.
[94] W.D. White, J.H. Malmberg and C.F. Driscoll, Phys. Rev. Lett., 49 (1982) 1822.
[95] J.D. Jackson, Classical Electrodynamics, Wiley, New York, 1975, Chap. 2.
[96] A.J. Peurrung and R.T. Kouzes, Int. J. Mass Spectrom. Ion Processes, (1995), in press.
[97] C. Roberson and C. Driscoll (eds.), Non-Neutral Plasma Physics, AIP, New York, 1988, p. 129.
[98] J. Notte and J. Fajans, Phys. Fluids, B (1994), in press.
[99] M.H. Holzscheiter et al., Nucl. Phys. A, 558 (1993) C709.
[100] T.G. Northrop, The Adiabatic Motion of Charged Particles, Wiley Interscience, New York, 1993.
[101] H. Goldstein, Classical Mechanics, Addison–Wesley, Menlo Park, 1980, p. 538.
[102] D. Nicholson, Plasma Theory, Wiley, New York, 1983, p. 29.
[103] J. Notte and J. Fajans, Phys. Rev. Lett., 70 (1993) 3900.
[104] T.M. O'Neil, Phys. Fluids, 23 (1980) 2216.
[105] T.M. O'Neil and R.A. Smith, Phys. Fluids B, 4 (1992) 2720.
[106] R.C. Davidson and N.A. Krall, Phys. Fluids, 13 (1970) 1543.
[107] S.A. Prasad and T.M. O'Neil, Phys. Fluids, 22 (1979) 278.
[108] T.M. O'Neil and C.F. Driscoll, Phys. Fluids, 22 (1979) 266.
[109] L.D. Landau and E.M. Lifshitz, Statistical Physics, Addison–Wesley, Reading, MA, 1969, p. 73.
[110] B.R. Beck, J. Fajans and J.H. Malmberg, Phys. Rev. Lett., 68 (1992) 317.
[111] C.F. Driscoll, Phys. Rev. Lett., 64 (1990) 645.
[112] T.J. Francl, E.K. Fukuda and R.T. McIver, Int. J. Mass Spectrom. Ion Processes, 50 (1983) 151.
[113] M.H. Douglas and T.M. O'Neil, Phys. Fluids, 21 (1978) 920.
[114] T.M. O'Neil, Phys. Fluids, 23 (1980) 725.
[115] L.D. Landau and E.M. Lifshitz, Statistical Physics, Addison–Wesley, Reading, MA, 1969, p. 11.
[116] A.J. Peurrung and J. Fajans, Phys. Fluids B, 5 (1993) 4250.
[117] D. Nicholson, Plasma Theory, Wiley, New York, 1983, Chap. 7.
[118] R. Chu, J.S. Wurtele, J. Notte, A.J. Peurrung and J. Fajans, Phys. Fluids B, 5 (1993) 2378.
[119] J. Notte, A.J. Peurrung, J. Fajans, R. Chu and J. Wurtele, Phys. Rev. Lett., 69 (1992) 3056.
[120] L.R. Brewer, J.D. Prestage, J.J. Bollinger, W.M. Itano, D.J. Larson and D.J. Wineland, Phys. Rev. A, 38 (1988) 859.
[121] D.H.E. Dubin, Phys. Rev. Lett., 66 (1991) 2076.
[122] J. Binney and S. Tremaine, Galactic Dynamics, Princeton University Press, Princeton, NJ, 1987, p. 247.
[123] S.A. Prasad and G.J. Morales, Phys. Fluids B, 1 (1989) 1329.
[124] T.M. O'Neil, Phys. Fluids, 24 (1981) 1447.
[125] W.L. Slattery, G.D. Doolen and H.E. DeWitt, Phys. Rev. A, 26 (1982) 2255.
[126] S. Ogata and S. Ichimaru, Phys. Rev. A, 36 (1987) 5451.
[127] D.H.E. Dubin, Phys. Rev. A, 42 (1990) 4972.
[128] J.H. Chu and I. Lin, Phys. Rev. Lett., 72 (1994) 4009.
[129] J.J. Bollinger, S.L. Gilbert, D.J. Heinzen, W.M. Itano and D.J. Wineland, in Strongly Coupled Plasma Physics, Elsevier,/Yamada Science Foundation, Amsterdam, 1990, p. 177.
[130] T.M. O'Neil, Phys. Rev. Lett., 55 (1985) 943.
[131] D.H.E. Dubin and T.M. O'Neil, Phys. Rev. Lett., 60 (1988) 1286.
[132] C.F. Driscoll, J.H. Malmberg and K.S. Fine, Phys. Rev. Lett., 60 (1988) 1290.
[133] J.H. Malmberg and C.F. Driscoll, Phys. Rev. Lett., 44 (1980) 654.
[134] D. Nicholson, Plasma Theory, Wiley, New York, 1983, p. 13.
[135] D.L. Book, NRL Plasma Formulary, revised, Office of Naval Research, Washington, DC, 1987.
[136] P.G. Hjorth and T.M. O'Neil, Phys. Fluids, 30 (1987) 2613.
[137] T.M. O'Neil, P.G. Hjorth, B. Beck, J. Fajans and J.H. Malmberg, in Strongly Coupled Plasma Physics, Elsevier, Amsterdam, 1990, p. 313.
[138] T. Hsu and J.L. Hirschfield, Rev. Sci. Instrum., 47 (1976) 236.
[139] R.H. Levy, Phys. Fluids, 8 (1965) 1288.
[140] C.F. Driscoll and K.S. Fine, Phys. Fluids B, 2 (1990) 1359.
[141] J.S. DeGrassie and J.H. Malmberg, Phys. Fluids, 23 (1980) 63.
[142] A.J. Peurrung, J. Notte and J. Fajans, Phys. Rev. Lett., 70 (1993) 295.
[143] S. Guan, X. Xiang and A.G. Marshall, Int. J. Mass Spectrom. Ion Processes, 124 (1993) 53.
[144] J.P. Speir, G.S. Gorman, C.C. Pitsenberger, C.A. Turner, P.P. Wang and I.J. Amster, Anal. Chem., 65 (1993) 1746.
[145] S.H. Guan and A.G. Marshall, J. Chem. Phys., 98 (1993) 4486.
[146] S. Guan, M.C. Wahl, T.D. Wood and A.G. Marshall, Anal. Chem., 65 (1993) 1753.
[147] M.P. Langevin, Ann. Chim. Phys., 5 (1905) 245.
[148] W.P. Allis, Handbuch Phys., 21 (1956) 383.
[149] T. Su and M.T. Bowers, J. Chem. Phys., 58 (1973) 3027.
[150] T. Su and M.T. Bowers, Int. J. Mass Spectrom. Ion Processes, 17 (1975) 309.
[151] W.J. Chesnavich, T. Su and M.T. Bowers, J. Chem. Phys., 72 (1980) 2641.
[152] D.R. Bates, Phys. Rev. A, 34 (1986) 1878.
[153] J. Troe, Chem. Phys. Lett., 122 (1985) 425.
[154] E.W. McDaniel, Collision Phenomena in Ionized Gases, Wiley, New York, 1964.
[155] C.F. Driscoll, in D. Cline (ed.), Low Energy Antimatter, World Scientific, Singapore, 1986, p. 184.
[156] A.J. Peurrung and J. Fajans, Phys. Fluids B, 5 (1993) 4295.

[157] P. Zaveri, P.I. John, K. Avinash and P.K. Kaw, Phys. Rev. Lett., 68 (1992) 3295.
[158] J.D. Jackson, Classical Electrodynamics, Wiley, New York, 1975, p. 659.
[159] D.J. Wineland and W.M. Itano, Phys. Rev. A, 20 (1979) 1521.
[160] W.M. Itano and D.J. Wineland, Phys. Rev. A, 25 (1982) 35.
[161] S. Stenholm, Rev. Mod. Phys., 58 (1986) 699.
[162] D.J. Wineland and W.M. Itano, Phys. Today, 40 (6) (1987) 34.
[163] J.J. Bollinger, D.J. Wineland and D.H.E. Dubin, Phys. Plas., 1 (1994) 1403.
[164] W. Kells, IEEE Trans. Nucl. Sci., NS32 (1985) 1770.
[165] D.J. Larson, J.C. Bergquist, J.J. Bollinger, W.M. Itano and D.J. Wineland, Phys. Rev. Lett., 57 (1986) 70.
[166] S.E. Barlow, Ph.D. Thesis, University of Colorado, Boulder, CO, 1984.
[167] V. Kovacik, J. Hirsch, D. Tholmann and H.F. Grutzmacher, Org. Mass Spectrom., 12 (1991) 1085.
[168] D. Tholmann, D. Flottmann and D. Grutzmacher, Chem. Ber., 124 (1991) 2349.
[169] L. Ngoka and C.B. Lebrilla, J. Am. Soc. Mass Spectrom., 4 (1993) 210.
[170] D.L. Eggleston, Bull. Am. Phys. Soc., 37 (1992) 1416.
[171] J. Notte and J. Fajans, Phys. Plas., 1 (1994) 1123.
[172] T.H. Stix, The Theory of Plasma Waves, McGraw–Hill, New York, 1962.
[173] R.H. Levy and R.W. Hockney, Phys. Fluids, 11 (1968) 766.
[174] R.J. Briggs, J.D. Dougherty and R.H. Levy, Phys. Fluids, 13 (1970) 421.
[175] L. Schweikhard and A.G. Marshall, J. Am. Soc. Mass Spectrom., 4 (1993) 433.
[176] C.S. Weimer, J.J. Bollinger, F.L. Moore and D.J. Wineland, Phys. Rev. A, 49 (1994) 3842.
[177] Y. Naito and M. Inoue, J. Mass Spectrom. Soc. Jpn., 42 (1994) 1.
[178] A.J. Peurrung and R.T. Kouzes, Int. J. Mass Spectrom., Ion Processes (1995).
[179] E.A. Cornell, R.M. Weisskoff, K.R. Boyce, R.W. Flanagan, G.P. Lafyatis and D.E. Pritchard, Phys. Rev. Lett., 63 (1989) 1674.
[180] D.J. Wineland and H.G. Dehmelt, J. Appl. Phys., 46 (1975) 919.
[181] M.M. Schauer, Ph.D. Thesis, University of Colorado, Boulder, CO, 1990.
[182] M.M. Schauer, S.R. Jefferts, S.E. Barlow and G.H. Dunn, J. Chem. Phys., 91 (1989) 4593.
[183] S.H. Lee, K.P. Wanczek and H. Hartmann, Adv. Mass Spectrom., 88 (1980) 1645.
[184] D.L. Rempel, E.B. Ledford, S.K. Huang and M.L. Gross, Anal. Chem., 59 (1987) 2527.
[185] D.J. Wineland and H.G. Dehmelt, Int. J. Mass Spectrom. Ion Processes, 16 (1975) 338.
[186] G. Savard et al., Phys. Lett. A, 158 (1991) 247.
[187] R. Chen and A.G. Marshall, Int. J. Mass Spectrom. Ion Processes, 133 (1994) 29.
[188] D. Nicholson, Plasma Theory, Wiley, New York, 1983, p. 127.
[189] D.H.E. Dubin, Phys. Fluids B, 5 (1993) 295.
[190] M.D. Tinkle, R.G. Greaves, C.M. Surko, R.L. Spencer and G.W. Mason, Phys. Rev. Lett., 72 (1994) 352.
[191] G. Dimonte, Phys. Rev. Lett., 46 (1981) 26.